



# Modern to millennium-old greenhouse gases emitted from ponds and lakes of the Eastern Canadian Arctic (Bylot Island, Nunavut)

F. Bouchard<sup>1,2,3</sup>, I. Laurion<sup>1,3</sup>, V. Prėskienis<sup>1,3</sup>, D. Fortier<sup>2,3</sup>, X. Xu<sup>4</sup>, and M. J. Whiticar<sup>5</sup>

<sup>1</sup>Centre Eau Terre Environnement, Institut national de la recherche scientifique, Québec, QC, G1K 9A9, Canada

<sup>2</sup>Département de géographie, Université de Montréal, Montréal, QC, H3C 3J7, Canada

<sup>3</sup>Centre d'études nordiques (CEN), Université Laval, Québec, QC, G1V 0A6, Canada

<sup>4</sup>Department of Earth System Science, University of California Irvine, Irvine, CA, 92697, USA

<sup>5</sup>Biogeochemistry Facility, School of Earth and Ocean Sciences, University of Victoria, Victoria, BC, V8W 3P6, Canada

Correspondence to: F. Bouchard (frederic.bouchard@cen.ulaval.ca)

Received: 1 July 2015 – Published in Biogeosciences Discuss.: 24 July 2015

Revised: 24 November 2015 – Accepted: 25 November 2015 – Published: 14 December 2015

**Abstract.** Ponds and lakes are widespread across the rapidly changing permafrost environments. Aquatic systems play an important role in global biogeochemical cycles, especially in greenhouse gas (GHG) exchanges between terrestrial systems and the atmosphere. The source, speciation and emission rate of carbon released from permafrost landscapes are strongly influenced by local conditions, hindering pan-Arctic generalizations. This study reports on GHG ages and emission rates from aquatic systems located on Bylot Island, in the continuous permafrost zone of the Eastern Canadian Arctic. Dissolved and ebullition gas samples were collected during the summer season from different types of water bodies located in a highly dynamic periglacial valley: polygonal ponds, collapsed ice-wedge trough ponds, and larger lakes. The results showed strikingly different ages and fluxes depending on aquatic system types. Polygonal ponds were net sinks of dissolved CO<sub>2</sub>, but variable sources of dissolved CH<sub>4</sub>. They presented the highest ebullition fluxes, 1 or 2 orders of magnitude higher than from other ponds and lakes. Trough ponds appeared as substantial GHG sources, especially when their edges were actively eroding. Both types of ponds produced modern to hundreds of years old (< 550 yr BP) GHG, even if trough ponds could contain much older carbon (> 2000 yr BP) derived from freshly eroded peat. Lakes had small dissolved and ebullition fluxes, however they released much older GHG, including millennium-old CH<sub>4</sub> (up to 3500 yr BP) from lake central areas. Acetoclastic methanogenesis dominated at all study sites and there was minimal, if any, methane oxidation in gas emitted through

ebullition. These findings provide new insights on GHG emissions by permafrost aquatic systems and their potential positive feedback effect on climate.

## 1 Introduction

Permafrost stores large quantities of carbon compared to the atmosphere, although quantitative estimates are still under discussion (Tarnocai et al., 2009; Hugelius et al., 2014). Climate warming impacts Arctic landscapes through permafrost thawing and erosion (Romanovsky et al., 2010). This results in the release of both old and recent organic carbon to the atmosphere as greenhouse gases (GHG) (Zimov et al., 2006; Schuur et al., 2015). Widespread across permafrost environments, aquatic systems act as biogeochemical hotspots by releasing substantial amounts of carbon dioxide (CO<sub>2</sub>) and methane (CH<sub>4</sub>) (e.g., Walter et al., 2007; Laurion et al., 2010; Abnizova et al., 2012). It is generally considered that CH<sub>4</sub> ebullition is the main mechanism of GHG emissions from ponds and lakes, a transport mechanism highly heterogeneous in space and time (Wik et al., 2011). However, other processes, such as emissions through diffusion (Bastviken et al., 2008), plant-mediated transport and microbial oxidation (Bastviken et al., 2004; Liebner et al., 2011), also need to be considered in the specific context of the Arctic. Moreover, lateral inputs of CH<sub>4</sub> produced within the active layer or lateral export of permafrost carbon away from thaw sites via streams and rivers were recently demonstrated (Vonk and

Gustafsson, 2013; Godin et al., 2014; Paytan et al., 2015). Overall, thermokarst (thaw) ponds and lakes represent a major landscape feature in permafrost-affected regions (Grosse et al., 2013), and there is a growing interest in defining the specific role of various types of freshwater ecosystems in global carbon dynamics associated to permafrost degradation, and how they may rapidly respond to environmental changes (see Vonk et al., 2015, and other articles in this special issue).

Upscaling and modeling GHG emissions is challenging, and oversimplified assumptions can lead to large calculation errors (Stepanenko et al., 2011; van Huissteden et al., 2011; Gao et al., 2013). The gaps that need to be fulfilled to model future GHG emissions with more accuracy include defining the vertical distribution of carbon in permafrost soils across the Arctic, the interactions between permafrost thaw and surface hydrology, as well as distinguishing CH<sub>4</sub> from CO<sub>2</sub> emissions and gradual warming from abrupt thaw mechanisms (Schuur et al., 2015). Regarding thermokarst systems specifically, aspects that should be further investigated include physical (e.g., heat transfer, diffusive GHG exchange, daily storage flux) and hydrological (e.g., surface and groundwater flows) dynamics, as well as fluxes of particulate and dissolved organic carbon to these systems (Vonk et al., 2015). Another important yet rarely considered aspect is the age (old vs. modern) of the carbon that is processed and released by these biogeosystems, which is linked to their potential to generate a positive feedback on climate (Walter et al., 2006; Vonk et al., 2013; Mann et al., 2015). Large GHG emissions (especially CH<sub>4</sub>) from old (late Pleistocene-age) organic ice-rich loess permafrost (*yedoma*) have been reported from thermokarst lakes of Siberia and Alaska in regions that were not ice-covered during the last glaciation (Zimov et al., 1997; Brosius et al., 2012). In Canada, which accounts for a very large portion of circum-Arctic permafrost, these deposits are rare as the territory was almost entirely covered by ice sheets during that period (Dyke and Prest, 1987). The carbon trapped in permafrost is thus younger (Holocene-age) in this part of the Northern Hemisphere (Allard, 1996; Burn and Kokelj, 2009; Lauriol et al., 2010; Tremblay et al., 2014). It nevertheless represents an excess carbon stock that can contribute to accelerate climate warming via a positive feedback mechanism if released as GHG, compared to modern carbon that is used and recycled through short-term biogeochemical processes (photosynthetic fixation and microbial respiration).

Preliminary data on GHG radiocarbon age from small tundra ponds on Bylot Island (Nunavut) in the Eastern Canadian Arctic showed that the carbon released by these systems was generally modern (Negandhi et al., 2013). The objective of the present study was to further characterize GHG composition, production pathway, age and emission rates in ponds and lakes at this particular site. We analyzed dissolved and ebullition gas samples collected in July from ponds and

lakes located within an organic-rich permafrost terrace of Late Holocene age (Fortier et al., 2006).

## 2 Study area

Bylot Island (Nunavut) is located in the Eastern Canadian Arctic, within the continuous permafrost zone (Fig. 1). The Byam Martin Mountains run southeast–northwest across the island, and the plains that stretch out on either side of the mountains belong to the Arctic Lowlands physiographic region (Bostock, 1970). The numerous valleys formed in the lowlands were shaped during the successive Pleistocene glaciations (Klassen, 1993). Since the Holocene, these valleys developed highly dynamic biogeosystems rich in permafrost ground ice, peat, and aquatic environments (Fortier and Allard, 2004). The study site (73°09' N; 79°58' W) is located in one such valley (glacier C-79) named Qarlikturvik, which has a NE-SW orientation and a surface area of ~65 km<sup>2</sup> (~15 km-long × 4–5 km-wide). A terminal moraine, located about halfway between the actual glacier front and the seashore and sitting on marine clay, was <sup>14</sup>C-dated to ~9.8 kyr BP (Allard, 1996). Glacial retreat, accompanied by a marine transgression phase, ended around 6 kyr BP. The clays were then covered by glacio-fluvial sand and gravels (Fortier and Allard, 2004). Today, a proglacial braided river runs through a glacio-fluvial outwash plain and drains glacier melt waters and sediments towards the Navy Board Inlet, where it forms a delta.

The outwash plain is bordered on both sides by a 3 to 5 m thick terrace, crisscrossed by networks of tundra polygons associated with the formation of syngenetic ice wedges (Figs. 1d and 2a). Along the southern bank of the river, the upper portion of the terrace is composed of alternating organic (peat) and mineral (wind-blown sand and silt) material, which started to accumulate over glacio-fluvial sands and gravels around 3700 years ago (Fortier and Allard, 2004). These peaty loess deposits contain excess pore ice (> 100 % dry weight) and their gravimetric organic matter content can reach over 50 %. The active layer depth in such deposits generally ranges between 40 to 60 cm, and the maximum depth of permafrost on Bylot Island has been estimated to be over 400 m (Smith and Burgess, 2000). The terrace comprises abundant aquatic systems of different sizes and shapes (Fig. 2) that can act as effective biogeochemical hotspots (Laurion et al., 2010; Negandhi et al., 2013). The hydrological network is mainly fed by rain and snowmelt runoff originating from gullies of the valley flanks or large snow banks on the lee side of hills. Most of water loss from ponds and lakes is through evaporation during the ice-free season (Negandhi, 2013).

The climate normal (1981–2010) is provided by a meteorological station located near the village of Pond Inlet (Mittimatalik) (72°41' N; 77°58' W), about 85 km southeast from the study site (Fig. 1c). The region has a polar climate

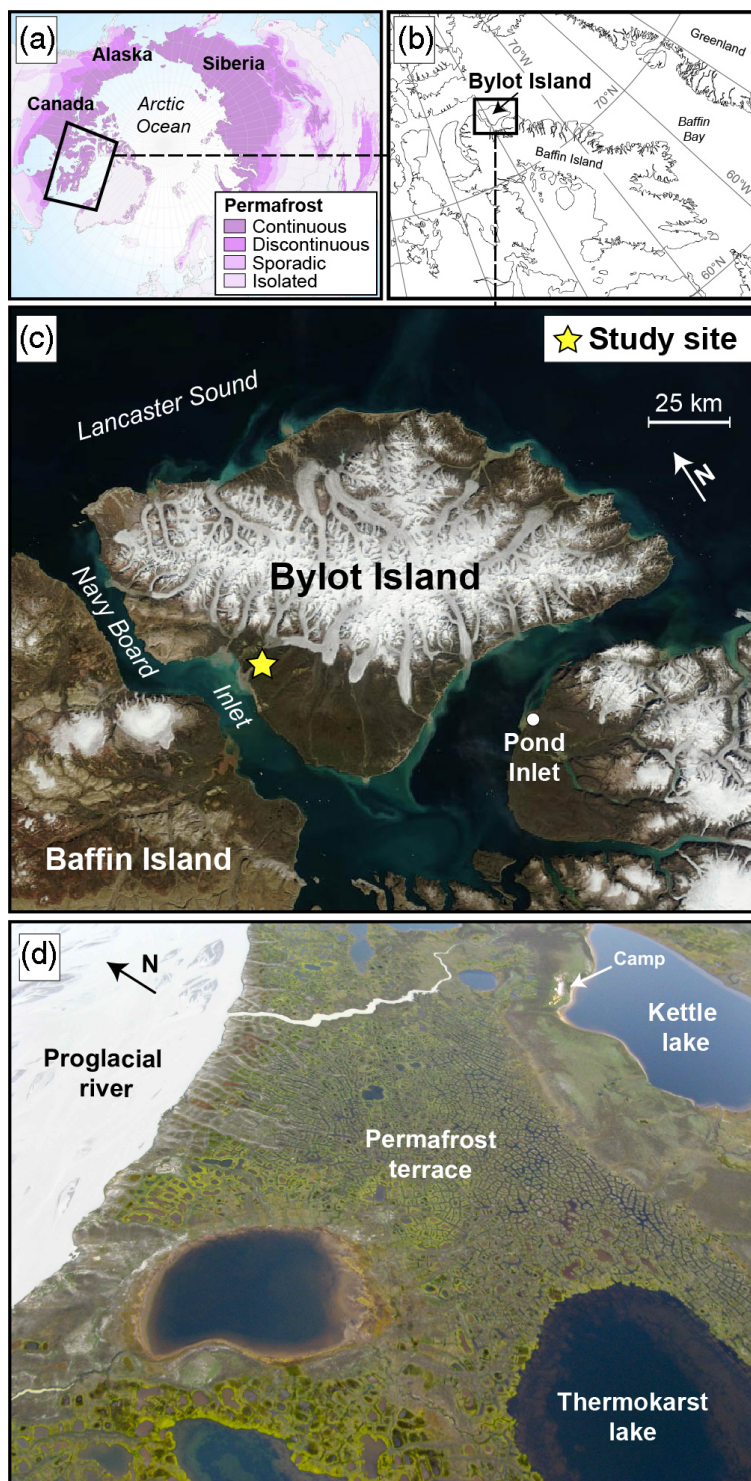


**Figure 1.** Location of the study site in the continuous permafrost zone of the Eastern Canadian Arctic (a), north of Baffin Island (b), within one of the several glacier valleys of Bylot Island, Nunavut (c). The studied valley contains numerous aquatic systems of different sizes (d). Source of the permafrost map (a): Brown et al. (1998). Satellite photo (c): Terra-MODIS, 22 July 2012.

with a slight marine influence, a mean annual air temperature of  $-14.6^{\circ}\text{C}$  (average daily temperatures ranging from  $-33.4^{\circ}\text{C}$  in January to  $6.6^{\circ}\text{C}$  in July) and total precipita-

tions of 189 mm, of which 91 mm fall as rain between June and September (Environment Canada, 2015). Thawing and freezing degree-days are around 475 and 5735, respectively.

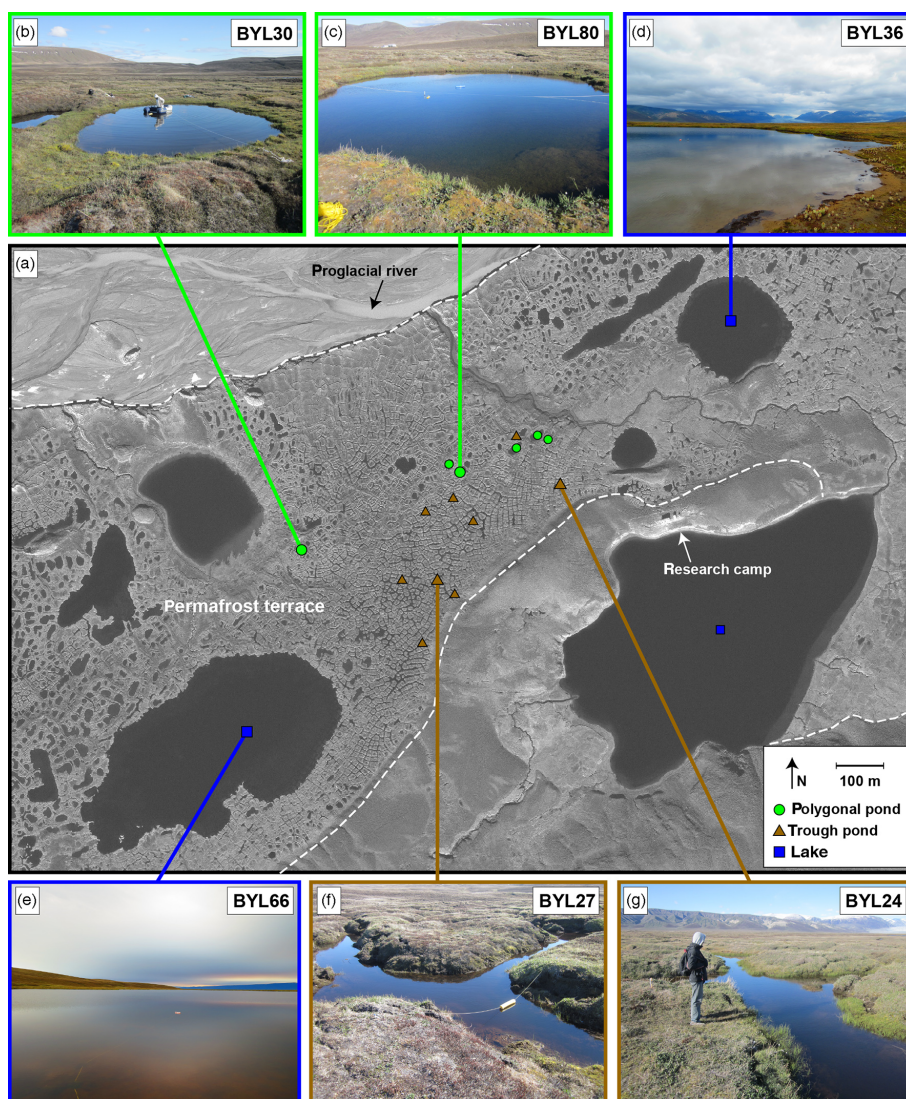


**Figure 2.** Location of the sampled water bodies (a), including polygonal ponds (b–c), kettle and thermokarst lakes (d–e, respectively) and trough ponds (f–g). Ponds and lakes are located within the limits of a peaty loess permafrost terrace, outlined with the dashed white line. Satellite photo (a): GeoEye-1, 18 July 2010.

Winter (continuous daily mean air temperature  $< 0^{\circ}\text{C}$ ) lasts from early September to mid-June, for an average total of 283 days per year. A station from the SILA network, operated since 2004 by the Center for Northern Studies (CEN) in the valley of glacier C-79, provides similar climate data (CEN, 2014).

The southwest plain of Bylot Island is a  $\sim 1600\text{ km}^2$  low-lying wetland area of graminoid-moss tundra (Parks Canada, 2014). Local vegetation in the Qarlikturvik valley is dominated by sedges (e.g. *Carex aquatilis* var. *stans*, *Eriophorum scheuchzeri*), grasses (e.g. *Arctagrostis latifolia*, *Dupontia fisheri*, *Pleuropogon sabinei*) and mosses (e.g. *Drepanocladus* spp., *Aulacomnium* spp.) (Duclos, 2002; Ellis et al., 2008).

### 3 Materials and methods

#### 3.1 Sampling sites

We selected and sampled different types of aquatic systems typical of the tundra polygon terrace of the valley (Fig. 2; Table 1): (1) polygonal ponds over low-centered ice wedge polygons; (2) elongated water channels over melting ice wedges (ponds formed in collapsed ice-wedge troughs, hereafter referred to as trough ponds); (3) lakes with underlying talik (unfrozen soil over permafrost), including a thermokarst (thaw) lake and a kettle (melted buried glacier ice) lake. A total of 23 ponds and lakes were sampled in June–July 2013, including 9 polygonal ponds, 12 trough ponds, and 2 lakes (1 thermokarst and 1 kettle lake). In July 2014, six water

**Table 1.** Limnological properties of ponds and lakes sampled in July 2013 and July 2014, including sampling depth, dissolved organic carbon (DOC), absorption coefficient of dissolved organic matter at 320 nm ( $a_{320}$ ), total phosphorus (TP), soluble reactive phosphorus (SRP), total nitrogen (TN), and selected major ions ( $\text{NO}_3$ ,  $\text{SO}_4$ , Fe). POL = polygonal pond; IWT = ice wedge trough pond; LAK = lake.

Site	Type	Depth m	DOC $\text{mg L}^{-1}$	$a_{320}$ $\text{m}^{-1}$	TP $\mu\text{g L}^{-1}$	SRP $\mu\text{g L}^{-1}$	TN $\text{mg L}^{-1}$	$\text{NO}_3$ $\text{mg L}^{-1}$	$\text{SO}_4$ $\text{mg L}^{-1}$	Fe $\text{mg L}^{-1}$
2013										
BYL30	POL	surf	8.7	17.8	14.8	NA	0.49	0.42	1.3	0.470
BYL80	POL	surf	5.6	9.0	22.9	NA	0.42	0.09	1.3	0.250
Average POL ( $n = 9$ )			6.7	12.7	17.6		0.47	0.17	1.3	0.282
BYL24	IWT	surf	6.6	27.0	16.1	NA	0.29	0.37	4.3	0.270
BYL27	IWT	surf	10.1	42.0	29.0	NA	0.58	0.07	6.2	1.400
Average IWT ( $n = 12$ )			10.0	38.0	27.8		0.63	0.19	6.7	1.014
BYL66	LAK	surf	4.2	16.4	20.7	NA	0.27	0.13	2.9	0.460
BYL36*	LAK	surf	3.9	5.8	16.2	0.33	0.22	0.10	1.7	0.067
2014										
BYL30	POL	surf	12.2	NA	8.5	1.31	1.32	0.25	2.6	0.648
BYL80	POL	surf	10.6	NA	22.7	1.75	1.25	< 0.2	1.6	0.266
BYL24	IWT	surf	8.8	NA	23.7	1.28	1.02	0.30	1.3	1.549
		0.9	9.3	NA	21.5	1.95	1.16	0.21	1.7	2.169
BYL27	IWT	surf	12.1	NA	27.4	1.56	1.22	0.29	2.7	0.487
		1.3	14.3	NA	54.8	1.41	1.70	0.25	2.4	2.979
BYL66	LAK	surf	4.3	NA	9.8	< 0.5	0.49	< 0.2	2.4	2.949
		2.0	4.2	NA	10.6	0.74	0.44	< 0.2	2.5	0.627
		4.5	4.1	NA	28.0	0.75	0.56	0.27	2.6	0.507
BYL36	LAK	surf	4.3	NA	6.7	1.13	0.45	0.27	2.2	0.023
		2.0	4.2	NA	NA	0.91	0.46	< 0.2	2.2	0.027
		10.0	4.2	NA	41.2	1.29	0.57	< 0.2	2.3	0.039

\* 2011 data

bodies (two polygonal ponds, two trough ponds, and two lakes including one thermokarst and one kettle lake) were selected and studied more intensively, including morphological measurements of ponds (depth, width and length) and lakes (bathymetry with a portable sonar as in Bouchard et al., 2015), and limnological profiles (see below).

### 3.2 Limnology

We measured a suite of limnological characteristics during both years, including temperature, dissolved oxygen, and concentrations of dissolved organic carbon (DOC), chromophoric fraction of dissolved organic matter (CDOM), nutrients (phosphorus, nitrogen) and major ions. Temperature and dissolved oxygen profiles were recorded with a ProODO handheld meter (YSI Inc.). Water samples were filtered through 0.2  $\mu\text{m}$  pre-rinsed cellulose acetate filters (2013) or pre-combusted GF/F filters (2014, nominal porosity 0.7  $\mu\text{m}$ ) to analyze DOC and major ions. Cations were fixed with  $\text{HNO}_3$  (0.15 % final concentration) while anions and DOC were not fixed but kept in dark and cold. DOC concentrations were measured with a Shimadzu TOC-5000A carbon analyzer calibrated with potassium biphthalate, and CDOM was quantified (in 2013 only) with the absorption

coefficient of DOM at 320 nm ( $a_{320}$ ) obtained on a Cary 300 (Varian; methodological details in Laurion and Mladenov, 2013). Major anions were quantified by ionic chromatography (Dionex ICS-2000), whereas major cations by inductively coupled plasma–optical emission spectrometry (ICP-OES, Varian VISTA AX). Total phosphorus (TP) and total nitrogen (TN) were quantified from unfiltered water samples fixed with  $\text{H}_2\text{SO}_4$  (0.15 % final concentration) as described by Stainton et al. (1977). Finally, the thermal structure of one trough pond (BYL27) was assessed during a full year (July 2013–July 2014) by recording water temperature at two depths (0 and 50 cm) at a 15 min interval using two submersible data loggers (Vemco Minilog-II-T, accuracy  $\pm 0.1$   $^\circ\text{C}$ , resolution  $\pm 0.01$   $^\circ\text{C}$ ) installed on a mooring line. The line was not moored at the deepest point of the pond ( $\sim 1$  m) as found upon its retrieval, but the data still provide a clear picture of the thermal stratification establishing in this type of humic ponds.

### 3.3 Ebullition flux of greenhouse gases

Ebullition gas samples were collected using submerged funnels (as in Wik et al., 2013) equipped with a 140 mL plastic syringe (Fig. A1 in Appendix A) and deployed for a

period of 1 h to 19 days depending on the flux. The samples trapped in the syringe were transferred into 50 mL glass bottles with butyl rubber stoppers (bottles acid-washed, pre-combusted, helium flushed and vacuumed) for  $^{14}\text{C}$  dating (see below), and into two separate 6 mL glass vials (helium flushed and vacuumed Exetainers) for stable isotope (see below) and gas chromatography analysis (Varian 3800, COMBI PAL head space injection system, CP PoraPLOT Q 0.53 mm ID  $\times$  25 m, flame ionization detector). Ebullition flux ( $F_e$ , in  $\text{mmol m}^{-2} \text{d}^{-1}$ ) was calculated as

$$F_e = (p_{\text{Gas}} \times V) / (A \times MV \times t),$$

where  $p_{\text{Gas}}$  is the partial pressure of  $\text{CO}_2$  or  $\text{CH}_4$ ,  $V$  is the collected gas volume,  $A$  is the funnel area,  $MV$  is the gas molar volume at ambient air temperature, and  $t$  is the collecting time.

### 3.4 Diffusive flux of greenhouse gases

Surface water dissolved GHG concentrations were obtained by equilibrating 2 L of lake or pond water with 20 mL of ambient air during 3 min (Hesslein et al., 1991). The resulting gaseous headspace was transferred into 6 mL glass vials and analyzed as above by gas chromatography. Dissolved GHG concentration at the surface ( $C_{\text{sur}}$ ) was calculated using Henry's law, and departure from saturation (sink vs. source) was calculated subtracting the gas concentration in the water at equilibrium with the atmosphere ( $C_{\text{eq}}$ , global values of atmospheric partial pressures from IPCC, 2007, were used). To estimate diffusive flux ( $\text{Flux}_d$ ), first the gas transfer coefficient ( $k_{600}$ ) standardized to a Schmidt number ( $Sc$ ) of 600 (Wanninkhof, 1992) was calculated with the wind-based model of Cole and Caraco (1998):

$$k_{600} = 2.07 + 0.215u_{10}^{1.7},$$

where  $u_{10}$  is the wind speed at 10 m above the ground, and then applying the equation:

$$\text{Flux}_d = k(C_{\text{sur}} - C_{\text{eq}}),$$

where  $k$  is the gas transfer coefficient for a given gas calculated as

$$k = k_{600}(Sc/600)^{-0.5}.$$

### 3.5 Radiocarbon analysis

Ebullition gas samples were analyzed at the Keck Carbon Cycle AMS facility at the University of California, Irvine. First,  $\text{CH}_4$  and  $\text{CO}_2$  were separated and purified by a zero air carrier gas flow-through line (Pack et al., 2015), and graphitized by the sealed tube Zn reduction method (Xu et al., 2007), then measured for radiocarbon ( $^{14}\text{C}$ ) on a compact accelerator mass spectrometer (AMS) (Southon and Santos, 2007). Data presented here are expressed as  $\Delta^{14}\text{C}$  (‰),

which is normalized to radiocarbon activity of an oxalic acid standard OX1 (decay corrected to 1950) and corrected for isotopic fractionation (Reimer et al., 2004).  $\Delta^{14}\text{C}$  (‰)  $> 0$  was further used to indicate “modern” carbon (1950 to present), and  $\Delta^{14}\text{C}$  (‰)  $< 0$  for “older” carbon (pre-1950). This was particularly helpful for polygonal and trough ponds, which provided modern or very young GHG. The  $\Delta^{14}\text{C}$  analytical error was  $\sim 2$  ‰ for modern sample, based on long-term measurements of secondary standards.  $^{14}\text{C}$  age (yr BP) is as defined by Stuiver and Polach (1977).

### 3.6 Stable isotope analysis

Stable carbon and hydrogen isotopic compositions of GHG,  $\delta^{13}\text{CO}_2$ ,  $\delta^{13}\text{CH}_4$ , and  $\delta\text{DCH}_4$ , were analyzed at the Biogeochemistry Facility School of Earth and Ocean Sciences (BF-SEOS, University of Victoria). Ebullition gas samples were analyzed for  $\delta^{13}\text{CH}_4$  by introducing the gas onto a GSQ PLOT column (0.32 mm ID, 30 m) using a Valco 6-port valve and sample loop. After chromatographic separation, the  $\text{CH}_4$  passes through an oxidation oven (1030 °C), a Nafion water trap, and open-split interface to a continuous flow-isotope ratio mass spectrometer (CF-IRMS). The  $\delta^{13}\text{CO}_2$  was measured similarly by CF-IRMS, but bypassing the combustion oven. Precision for the  $\delta^{13}\text{CH}_4$  and  $\delta^{13}\text{CO}_2$  analyses was  $\pm 0.2$  ‰, relative to Vienna PeeDee Belemnite (VPDB). Hydrogen isotope ratios of  $\text{CH}_4$  ( $\delta\text{DCH}_4$ ) were measured by a TC/EA pyrolysis unit (1450 °C) interfaced to a CF-IRMS. Precision for the  $\delta\text{DCH}_4$  analyses was  $\pm 3$  ‰, relative to Vienna Standard Mean Ocean Water (VSMOW). Carbon and hydrogen isotope ratios are expressed using standard delta ( $\delta$ ) notation as described by deviations from a standard such that

$$\delta_{\text{sample}} \text{‰} = [(R_{\text{sample}}/R_{\text{standard}}) - 1] \times 1000,$$

where  $R$  is the  $^{13}\text{C}/^{12}\text{C}$  or  $^2\text{H}/^1\text{H}$  ratio in the sample or standard. For isotope calibration, methane carbon and hydrogen standards from Isometric Instruments were used. These are traceable back to VPDB for carbon isotope ratios and VSMOW for hydrogen isotope ratios.

## 4 Results

### 4.1 Morpho-limnological properties of ponds and lakes

Ponds were generally shallow ( $\sim 0.6$ – $1.0$  and  $1.0$ – $1.5$  m deep for polygonal and trough ponds, respectively) and thus froze to the bottom during winter, whereas lakes were more variable in depth depending on their origin and at least a portion of them did not freeze to the bottom in winter. The thermokarst lake was a few meters deep ( $< 5$  m), while the kettle lake was deeper ( $< 12$  m). Polygonal ponds, including different developmental stages and coalesced ponds, generally had flat bottoms covered by cyanobacterial mats (up

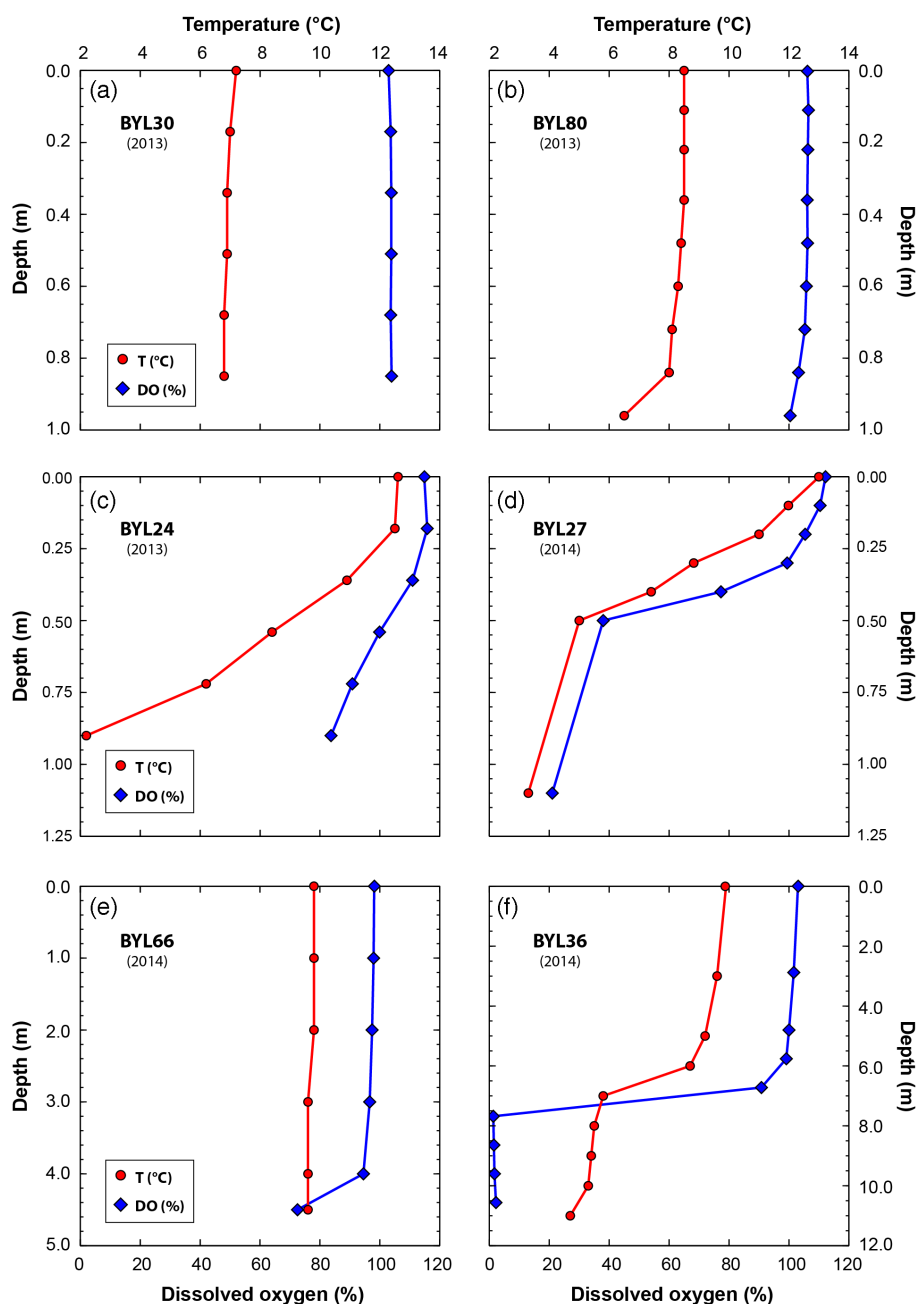


**Figure 3.** Temperature (°C; upper x axes) and dissolved oxygen (%; lower x axes) profiles for polygonal ponds BYL30 (a) and BYL80 (b), trough ponds BYL24 (c) and BYL27 (d), and lakes BYL66 (e) and BYL36 (f). Some profiles (a–c) were taken in July 2013, whereas the others (d–f) were taken in July 2014. Note the different vertical scales (depth).

to 5 cm thick), and stable (non-eroding) shores (Fig. 2b, c). Their surface area varied substantially (from 21 to 3350 m<sup>2</sup>) with a median of around 160 m<sup>2</sup>. Trough ponds were elongated water channels (median width ~ 3 m; median length ~ 10 m), and their shores were either actively eroding with collapsing decimetric peat blocks (Fig. 2f), or stable and colonized by brown mosses (Fig. 2g). The thermokarst lake had sharp edges near the shore, a shallow and gently sloping lake

bottom and a deeper central basin. The kettle lake had steeper slopes along its margins, and showed a deep section that was not in the center of the lake (Bouchard et al., 2015).

Ponds and lakes showed contrasting physicochemical conditions during the 2 sampling years (Table 1). Trough ponds generally had the highest concentrations of DOC, nutrients and ions, followed by polygonal ponds, whereas lakes showed the lowest values. Trough pond BYL27, where shore

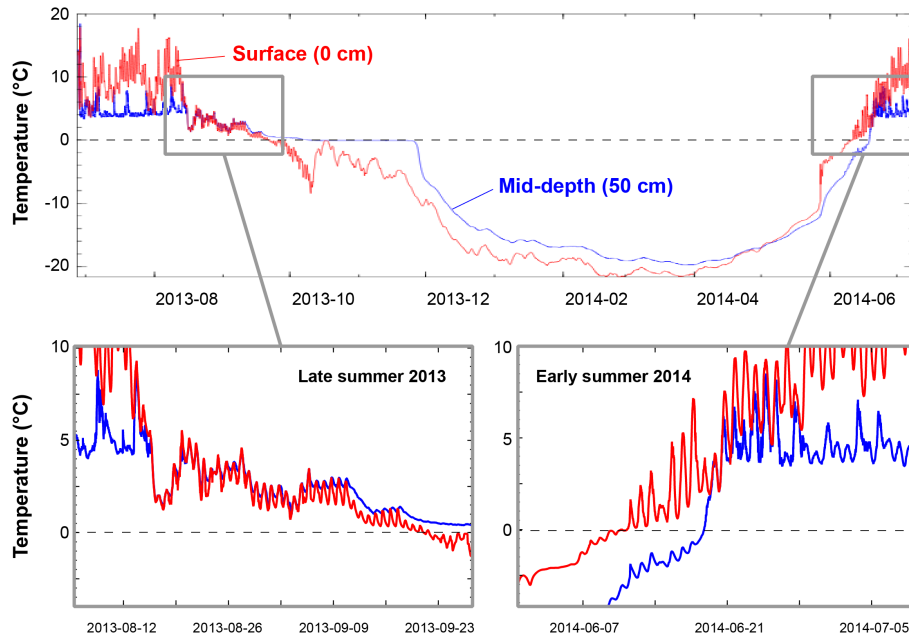


**Figure 4.** Water temperature at two depths (surface = 0 cm; mid-depth = 50 cm) in trough pond BYL27 over 1 year (27 June 2013 to 8 July 2014), showing extended stratification and rare mixing events (lower panels) during the summer.

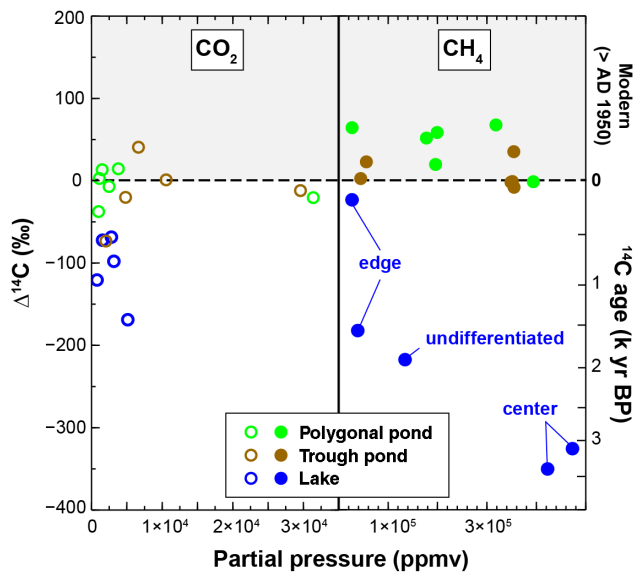


**Figure 5.** Concentration and age of ebullition GHG collected from ponds and lakes on Bylot Island, Nunavut. Gas concentration ( $x$  axis) is expressed as partial pressure (in ppmv, parts per million volumetric) of  $\text{CO}_2$  (open circles) and  $\text{CH}_4$  (full circles). Radiocarbon age is expressed as the normalized radiocarbon activity ( $\Delta^{14}\text{C}$ , in ‰; left  $y$  axis) corrected for isotopic fractionation and decay that took place between sampling and measurement dates, and in thousands of years before present (kyr BP; right  $y$  axis).

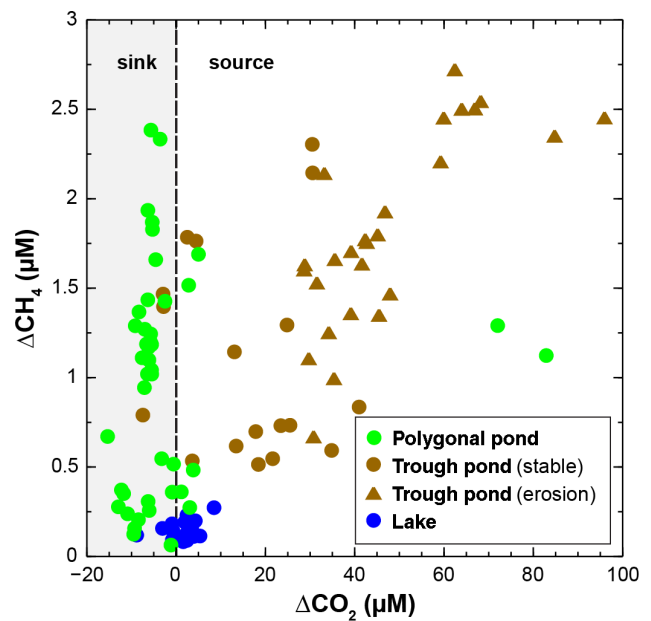


**Figure 6.** Saturation levels of dissolved GHG in pond and lake water. Values are expressed as the departure from saturation (in  $\mu\text{M}$ ) for  $\text{CO}_2$  ( $x$  axis) and  $\text{CH}_4$  ( $y$  axis). Values  $< 0$  indicate a sink, whereas values  $> 0$  indicate a source.

erosion was active during summer time, had near- or higher-than-average concentrations, whereas trough pond BYL24,

with stable shores, showed lower-than-average values. Pond DOC, nutrient and ion concentrations were substantially higher in 2014, a particularly dry year (total precipitations from January to June = 27.0 mm in 2014, compared to

50.7 mm in average; Table B1 in Appendix B), with resulting low pond water levels as observed in the field. When considering specific solute species separately, all of them except  $\text{NO}_3^-$  and  $\text{SO}_4^{2-}$  were statistically different ( $p < 0.0001$ ) among aquatic system types in 2013. In contrast, in 2014 only DOC ( $p < 0.0001$ ), total nitrogen (TN,  $p < 0.001$ ) and soluble reactive phosphorus (SRP,  $p < 0.05$ ) showed significant differences, and only between lakes and ponds (i.e., not between polygonal and trough ponds). Among all the water chemical properties and regardless of the sampling year, DOC showed the highest statistical contrasts between the different types of water bodies.

Polygonal ponds (BYL30, BYL80) had a thermally homogenous and well-oxygenated water column in July, whereas trough ponds (BYL24, BYL27) were notably stratified (Figs. 3 and 4). Thermokarst lake BYL66 was relatively well mixed over most of the water column, except near the sediment-water interface where dissolved oxygen decreased rapidly. Kettle lake BYL36, deeper than the other sampled water bodies, showed a steep gradient between the warmer, well-oxygenated epilimnion and the much colder, anoxic hypolimnion. The thermal profiles on Fig. 3 are representative of the conditions generally prevailing from July to mid August in each type of water bodies.

#### 4.2 Age and concentration of greenhouse gases released through ebullition

Radiocarbon age ( $\Delta^{14}\text{C}$  signature) and concentration of GHG ( $\text{CO}_2$  and  $\text{CH}_4$ ) emitted through ebullition showed strikingly different trends between the various types of aquatic systems (Fig. 5). Polygonal and trough ponds produced modern  $\text{CH}_4$  and modern to a few hundred years old ( $< 550$  yr BP)  $\text{CO}_2$ , whereas lakes generally released older GHG, ranging from 510 to 1425 yr BP for  $\text{CO}_2$  and from 125 to 3405 yr BP for  $\text{CH}_4$  (Table 2). Moreover, samples from lake edges had younger and less concentrated  $\text{CH}_4$  than those coming from lake central area. No such trend was observed for  $\text{CO}_2$  in lakes. Considering all ponds and lakes as a whole,  $\text{CH}_4$  was generally 1 to 2 orders of magnitude more concentrated than  $\text{CO}_2$  in emitted bubbles in July.

#### 4.3 Dissolved and ebullition fluxes of greenhouse gases

Polygonal ponds were generally  $\text{CO}_2$  sinks, but they were  $\text{CH}_4$  sources with a relatively broad range of saturation levels ( $\sim 0$ – $2.4 \mu\text{M}$ ) (Fig. 6). Lakes were near the equilibrium with the atmosphere (all samples clustered near 0 for both gases), being small sinks or sources of  $\text{CO}_2$ , and small sources of  $\text{CH}_4$ . Trough ponds were in general supersaturated in both gases, especially when their margins were actively eroding (highest GHG saturation values) (Fig. C1). Trough ponds showed the highest diffusive flux, especially of  $\text{CO}_2$  ( $65.5 \text{ mmol m}^{-2} \text{ d}^{-1}$ ; Table 3) with a median diffusive  $\text{CO}_2$  flux ( $21.8 \text{ mmol m}^{-2} \text{ d}^{-1}$ ) more than 12

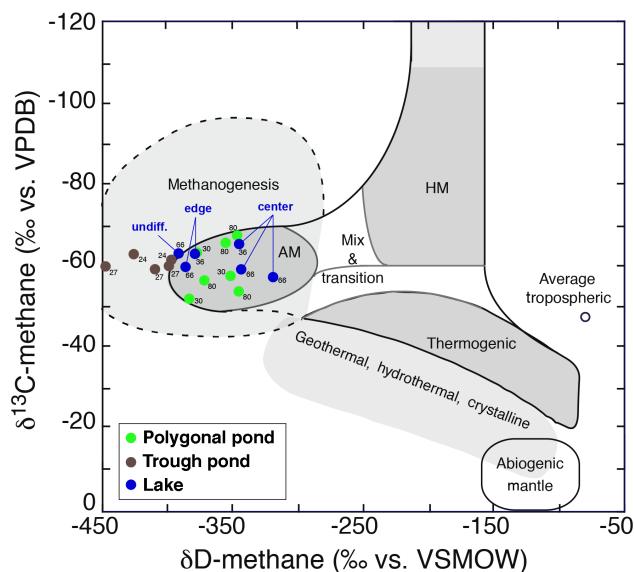


**Figure 7.** Carbon ( $\delta^{13}\text{C}$ ) and hydrogen ( $\delta\text{D}$ ) isotope composition of the methane emitted through ebullition by the sampled ponds and lakes, after Whiticar et al. (1986). AM = acetoclastic methanogenesis; HM = hydrogenotrophic methanogenesis; undiff. = undifferentiated lake sample location (edge vs. center).

times higher than the median value of all sampled water bodies ( $1.7 \text{ mmol m}^{-2} \text{ d}^{-1}$ ). Polygonal ponds, on the other hand, showed the highest ebullition flux for both  $\text{CO}_2$  ( $16.3 \text{ mmol m}^{-2} \text{ d}^{-1}$ ) and  $\text{CH}_4$  ( $534.5 \text{ mmol m}^{-2} \text{ d}^{-1}$ ), with a median ebullition  $\text{CH}_4$  flux that, although relatively low ( $\sim 1.0 \text{ mmol m}^{-2} \text{ d}^{-1}$ ), was  $\sim 5$  times higher than the median value for all ponds and lakes ( $\sim 0.2 \text{ mmol m}^{-2} \text{ d}^{-1}$ ). Lakes generally showed the lowest fluxes (both diffusion and ebullition). Globally, diffusion appeared as the dominant mechanism for  $\text{CO}_2$  emission, whereas  $\text{CH}_4$  was mainly emitted through ebullition. Statistical tests ran on the GHG data showed that trough ponds (BYL24, BYL27) were significantly different ( $p < 0.001$ ) from the other two types of water bodies (polygonal ponds and lakes), but also from each other. Furthermore, dissolved  $\text{CO}_2$  and  $\text{CH}_4$  fluxes were significantly correlated ( $p < 0.006$ ) with CDOM ( $r = 0.79$  and  $0.78$ , respectively;  $N = 22$ ;  $a_{320}$  only available in 2013), but only  $\text{CH}_4$  fluxes were correlated ( $p < 0.003$ ) with DOC ( $R = 0.61$ ,  $N = 28$ ; data available in both years).

#### 4.4 Carbon and hydrogen stable isotope ratios in ebullition gas samples

The stable isotope ratios of methane ( $\delta^{13}\text{CCH}_4$ ,  $\delta\text{DCH}_4$ ) and carbon dioxide ( $\delta^{13}\text{C}\text{CO}_2$ ) were measured on 18 ebullition samples collected in 2013 and 2014 (Table 2; Figs. 7 and 8). The  $\delta^{13}\text{CCH}_4$  average values were  $-60.5 \text{ ‰}$  and ranged from  $-52.1 \text{ ‰}$  to the most  $^{13}\text{C}$ -depleted value of  $-67.6 \text{ ‰}$ , both from polygonal ponds. The  $\delta\text{DCH}_4$  values, which averaged  $-376.80 \text{ ‰}$ , were relatively  $^2\text{H}$ -depleted for naturally

**Table 2.** Greenhouse gas radiocarbon and stable isotope results for the six priority ponds and lakes sampled during 2 consecutive years (2013 and 2014). Active layer samples collected in 2013 near two trough ponds are also included. POL = polygonal pond; IWT = ice wedge trough pond; LAK = lake; UAL = upper active layer (0–5 cm); LAL = lower active layer (50–60 cm); Fm = fraction modern.

Year	Site	Type	Gaseous	Gaseous	Fm	Fm	$\Delta^{14}\text{C}$	$\Delta^{14}\text{C}$	$^{14}\text{C}$ age	$^{14}\text{C}$ age	$\delta^{13}\text{C}$	$\delta^{13}\text{C}$	$\delta\text{D}$
			$\text{CO}_2$	$\text{CH}_4$	$\text{CO}_2$	$\text{CH}_4$	$\text{CO}_2$	$\text{CH}_4$	$\text{CO}_2$	$\text{CH}_4$	vs. VPDB	vs. VPDB	vs. VSMOW
2013	BYL30	POL	2580	324066	1.022	1.060	14	52	> Modern	> Modern	-10.6	-63.3	-378
2013	BYL80	POL	29124	784232	1.001	1.027	-7	20	0	> Modern	0.3	-67.6	-347
2013	BYL80	POL	735	234455	0.987	1.006	-21	-1	105	> Modern	-13.7	-65.7	-356
2013	BYL24	IWT	5783	115383	0.987	1.031	-20	23	105	> Modern	-21.8	-61.5	-398
2013	BYL27	IWT	1542	77007	0.934	1.010	-73	2	550	> Modern	-17.4	-60.1	-399
2013	BYL66	LAK	5269	324781	0.837	0.788	-169	-218	1425	1910	-8.4	-63.2	-392
2014	BYL30	POL	1607	18406	1.021	1.073	13	64	Modern	> Modern	-18.1	-57.7	-352
2014	BYL30	POL	2857	15724	NA	NA	NA	NA	NA	NA	-16.2	-52.1	-384
2014	BYL80	POL	< 50	174762	1.010	1.067	3	58	Modern	Modern	NA	-53.9	-346
2014	BYL80	POL	< 50	232178	0.970	1.076	-38	68	245	> Modern	NA	-56.5	-372
2014	BYL24	IWT	< 50	330145	1.049	1.043	41	35	Modern	Modern	NA	-63.0	-426
2014	BYL27	IWT	32383	291005	0.996	1.000	-12	-8	35	5	-16.1	-59.3	-410
2014	BYL27	IWT	< 50	251821	1.009	1.006	1	-2	Modern	Modern	NA	-59.9	-448
2014	BYL66	LAK	1774	31124	0.935	0.824	-72	-182	540	1555	-17.9	-59.9	-387
2014	BYL66	LAK	< 50	436334	0.909	0.680	-98	-326	765	3105	NA	-59.2	-344
2014	BYL66	LAK	< 50	330116	0.939	0.655	-69	-350	510	3405	NA	-57.4	-320
2014	BYL36	LAK	< 50	25187	0.886	0.984	-121	-23	970	125	NA	-63.1	-379
2014	BYL36	LAK	3845	1761	NA	NA	NA	NA	NA	NA	-17.5	-65.5	-345
2013	BYL27 (UAL)	IWT	n/a	n/a	1.062		62		> Modern		-28.9		NA
2013	BYL27 (LAL)	IWT	n/a	n/a	0.730		-270		2535		-26.3		NA
2013	BYL28 (UAL)	IWT	n/a	n/a	1.000		-1		5		NA		NA
2013	BYL28 (LAL)	IWT	n/a	n/a	0.759		-241		2210		NA		NA

**Table 3.** Diffusive and ebullition fluxes of  $\text{CO}_2$  and  $\text{CH}_4$  for the six priority ponds and lakes sampled during 2 consecutive years (2013 and 2014). POL = polygonal pond; IWT = ice wedge trough pond; LAK = lake; Min = minimum; Med = median; Max = maximum.

Site	Type	N	Diffusive fluxes ( $\text{mmol m}^{-2} \text{d}^{-1}$ )						Ebullition fluxes ( $\text{mmol m}^{-2} \text{d}^{-1}$ )						
			$\text{CO}_2$			$\text{CH}_4$			$\text{CO}_2$			$\text{CH}_4$			
			Min	Med	Max	Min	Med	Max	Min	Med	Max	Min	Med	Max	
BYL30	POL	12	-8.11	-1.04	5.73	0.19	1.07	1.46	12	0.00	0.01	0.26	0.01	0.89	26.57
BYL80	POL	32	-11.78	-3.14	45.44	0.03	0.53	1.14	9	0.00	0.00	16.32	0.11	0.99	534.54
BYL24	IWT	18	-5.44	13.27	26.30	0.05	0.17	1.51	8	0.00	0.00	0.02	0.01	0.06	0.29
BYL27	IWT	26	15.96	25.86	65.50	0.34	1.03	5.82	11	0.00	0.00	5.18	0.00	4.55	32.93
BYL66	LAK	12	-7.05	1.62	5.13	0.06	0.09	0.27	11	0.00	0.00	0.00	0.00	0.15	5.08
BYL36	LAK	6	-0.75	1.20	1.37	0.06	0.08	1.13	2	0.00	0.00	0.00	0.00	0.02	0.03
All water bodies		106	-11.78	1.74	65.50	0.03	0.54	5.82	53	0.00	0.00	16.32	0.00	0.18	534.54

occurring methane. The  $\delta\text{DCH}_4$  with the most  $^2\text{H}$ -enriched value came from the thermokarst lake sample collected at its center ( $-319.56\text{‰}$ ; BYL66; Fig. 7). In contrast, the  $\delta\text{DCH}_4$  values from trough ponds (BYL24 and BYL27) were consistently and extremely  $^2\text{H}$ -depleted, with values from  $-397.7\text{‰}$  to a very low value of  $-448.1\text{‰}$ . There was no apparent correspondence between the methane concentration and  $\delta^{13}\text{CH}_4$  or  $\delta\text{DCH}_4$ . The  $\text{CO}_2$  contents of ebullition samples were sometimes insufficient for carbon isotope measurements. For those with more  $\text{CO}_2$ , the average  $\delta^{13}\text{CO}_2$  was  $-14.3\text{‰}$  and varied from  $+0.3$  (polygonal pond BYL80) to  $-21.8\text{‰}$  (trough pond BYL24). There was also no apparent correspondence between the  $\text{CO}_2$  concentration and  $\delta^{13}\text{CO}_2$ .

However, it is worth noting that the sample with the most  $^{13}\text{C}$ -enriched  $\text{CO}_2$  also corresponded to the one with the most  $^{13}\text{C}$ -depleted  $\text{CH}_4$  (polygonal pond BYL80; Fig. 8).

## 5 Discussion

### 5.1 The strong heterogeneity in greenhouse gas age and concentration

We observed large variability in the age, composition and emission rate of GHG released by the studied aquatic systems. The GHG escaping through ebullition ranged from modern to a few centuries old for polygonal and trough ponds,

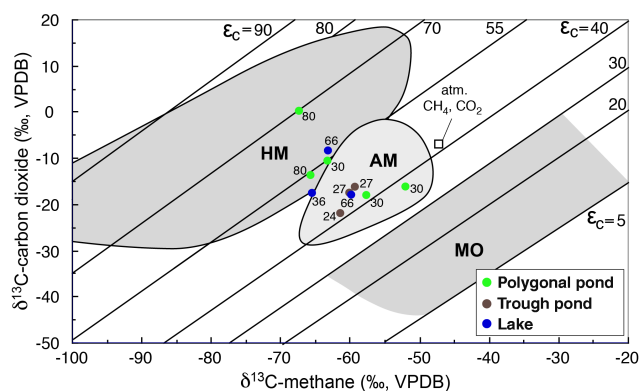


**Figure 8.** Carbon isotope composition ( $\delta^{13}\text{C}$ ) of  $\text{CH}_4$  (x axis) and  $\text{CO}_2$  (y axis) emitted by the sampled ponds and lakes. HM = hydrogenotrophic methanogenesis; AM = acetoclastic methanogenesis; MO = methane oxidation.

and from a few centuries to a few millennia old for lakes (Fig. 5). Trough ponds emitted slightly but significantly older  $\text{CH}_4$  than polygonal ponds ( $\Delta^{14}\text{C} = 10 \pm 18 \text{‰}$  vs.  $43 \pm 28 \text{‰}$ , respectively;  $p < 0.05$ ), as observed earlier at the same site (Negandhi et al., 2013), although still classified as modern carbon, suggesting a small contribution of peat-derived carbon pool to microbial activity in trough ponds. Surprisingly, trough ponds did not emit millennium-old  $\text{CH}_4$ , at least in July, despite the fact that they were exposed to eroding peat from down to the base of the active layer in the surroundings ( $^{14}\text{C}$  dates ranging from  $\sim 2.2$  to  $2.5$  kyr BP; Table 2) and even older peat strata up-thrusted along ice wedges by cryoturbation and now in contact with surface waters (Fortier and Allard, 2004). Eroding peat was likely leaching old carbon into the water column, but bottom sediment interstitial water, where  $\text{CH}_4$  is mostly produced, did not predominantly emit carbon of this age. Permafrost disturbance was indeed shown to deliver millennia-old particulate organic carbon and DOC to arctic streams and rivers (Lamoureux and Lafrenière, 2014; Guo et al., 2007; Vonk et al., 2013), acting as a significant source of bioavailable carbon in Arctic freshwaters (Mann et al., 2015). We speculate that microbes were preferably using young carbon, putatively more labile and more abundant at this time of the year, and may use older carbon stocks later when primary producers are less active. If the  $\text{CH}_4$  released from trough ponds is indeed older during the autumn and spring, this could represent a positive climate feedback, but our results now indicate a limited role.

On the other hand,  $\text{CH}_4$  ebullition samples collected from lakes provided older dates, up to nearly 3500 yr BP (thermokarst lake BYL66), which is very close to the maximum known age of the permafrost peat layers in the valley ( $3670 \pm 110$  yr BP; Fortier and Allard, 2004). It may suggest that permafrost thaw underneath this lake has proceeded through the organic layers at this site, which could result in decreased emissions in the future after the microbial exhaus-

tion of the labile fraction of the organic matter pool (Walter et al., 2007). However the timing of this reduction is unknown. We observed a spatial gradient in the age and concentration of  $\text{CH}_4$  in bubbles emitted from the thermokarst lake, with younger and less concentrated  $\text{CH}_4$  from the lake edge ( $\sim 3 \text{‰}$ ), and older and more concentrated  $\text{CH}_4$  from the center (up to  $57 \text{‰}$ ). The development of a talik (unfrozen soil under lake) explains the mobilization of deeper and older  $\text{CH}_4$  at the lake center where water remains unfrozen under the ice cover in winter (maximum lake depth  $> 4$  m, ice cover thickness  $\sim 2$  m). Methane emitted from a given location would thus be composed of a mixture of young  $\text{CH}_4$  from the edge with older  $\text{CH}_4$  from the center (Fig. D1). To our knowledge, the only other studies of thermokarst lakes presenting  $^{14}\text{C}$  dates on GHG are in *yedoma* deposits (Alaska, Siberia), which have very different ground ice, sediment and organic carbon contents, and chronostratigraphic history. For these lakes, the release of very old ( $> 40$  kyr BP) and highly concentrated (up to  $90 \text{‰}$ )  $\text{CH}_4$  from deep unfrozen lake sediments has been found (Walter et al., 2008). However, this study also reported younger ages for ebullition samples emitted from different parts of the lakes, and generally younger towards the lake center (when from background ebullition). At our study site, even though older GHG were emitted from lakes compared to ponds, ebullition fluxes remained low during the study period (July). Walter-Anthony and Anthony (2013) concluded that the classic randomized bubble-trap method for estimating mean lake ebullition is highly median-biased toward underestimation of fluxes, and this was possibly also occurring for our data set, although no systematic point source studies have been conducted so far at our study site.

We also observed strong differences in dissolved GHG flux depending on pond and lake types (Fig. 6; Table 3): polygonal ponds were  $\text{CO}_2$  sinks but  $\text{CH}_4$  sources while trough ponds were significant sources of both GHG, as previously reported in the valley (Laurion et al., 2010; Negandhi et al., 2013), and lakes were small sources of GHG. This pattern can be explained by the morpho-limnological properties of the water bodies. Polygonal ponds had stabilized shores (no apparent slumping) and more transparent waters compared to other systems, as shown by their lower CDOM content (Laurion et al., 2010). Moreover, they had flat and shallow bottoms covered by abundant cyanobacterial mats actively photosynthesizing and acting as a relatively efficient  $\text{CO}_2$  sink (flux reaching  $-11.8 \text{ mmol m}^{-2} \text{ d}^{-1}$ ). This is however 1 order of magnitude lower than the net ecosystem  $\text{CO}_2$  uptake measured over the summer from a wet polygonal tundra site in Siberia (flux reaching  $-104.7 \text{ mmol m}^{-2} \text{ d}^{-1}$ ; Kutzbach et al., 2007). Bottom sediments of the studied polygonal ponds were also colonized by methanotrophic bacteria (Negandhi et al., 2014), which can be a significant control mechanism on  $\text{CH}_4$  emissions as shown in polygonal ponds of the Lena region (Liebner et al., 2011).

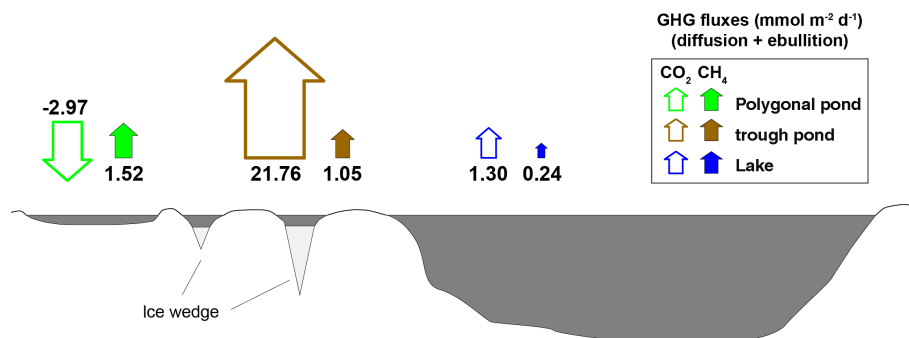


**Figure 9.** Schematic diagram of median fluxes of CO<sub>2</sub> and CH<sub>4</sub> from each type of water body in July. Note that dissolved and ebullition fluxes are combined (see Table 3 for details).

Lakes were larger and deeper, thus they were exposed to wind-induced mixing of their epilimnetic waters promoting venting of the GHG from this layer. When the water column is seasonally stratified (like in BYL36), the hypolimnion likely stores a large fraction of the GHG produced by the lake until the autumnal overturn period (Bastviken et al., 2004), allowing more space and time for the oxidation of dissolved CH<sub>4</sub>, and for the dissolution of a fraction of ebullition CH<sub>4</sub> (Bastviken et al., 2008). Therefore, it is possible that higher flux of old carbon would be observed later in the season. To fully account GHG emissions from lakes and compare them to other aquatic systems, summer and winter storage fluxes will need to be estimated (Boereboom et al., 2012; Langer et al., 2015; Walter-Anthony et al., 2010; Wik et al., 2011).

Trough ponds presented the highest combined (CO<sub>2</sub> + CH<sub>4</sub>; diffusion + ebullition) GHG fluxes at the time of sampling (Fig. 9). Considering a global warming potential (GWP) of 34 for CH<sub>4</sub> on a 100-year horizon (Myhre et al., 2013), trough ponds presented the highest net carbon efflux (1.5 g CO<sub>2</sub>-equivalent m<sup>-2</sup> d<sup>-1</sup>, compared to 0.7 and 0.2 g CO<sub>2</sub>-equivalent respectively for polygon ponds and lakes). Despite their shallow depths, trough ponds were strongly stratified with oxygen-depleted and cold bottom waters. The bottom temperature in these ponds was indeed near 0 °C (Fig. 3) because this layer of water is lying just above the melting ice wedge (as part of the active layer), it does not mix with surface waters and it is cooled down through sensible heat transfer. Moreover, trough ponds were not colonized by photosynthesizing (CO<sub>2</sub> sink) and methanotrophic (CH<sub>4</sub> sink) bacteria such as in polygonal ponds (Negandhi et al., 2014). Stronger water column hypoxia generated anoxia more rapidly in the sediments, and the organic material inputs caused by active erosion likely led to higher CH<sub>4</sub> production, although the young carbon signature of emitted CH<sub>4</sub> is still puzzling (see below). Meanwhile, the eroding conditions and reduced light availability (higher CDOM, TP and turbidity; Table 1) in trough ponds favored net heterotrophy and net CO<sub>2</sub> emissions, as found in subarctic thermokarst lakes (Roiha et al., 2015). Similar to polygo-

nal ponds, the shallow depth of trough ponds reduces the chances for dissolution of CH<sub>4</sub> bubbles into the water column and its subsequent oxidation before reaching the atmosphere. Moreover, the thermal structure of trough ponds (low transparency, microtopography) can impede mixing for several weeks (Fig. 4), thus favoring GHG summer storage in bottom waters, and likely generating stronger diffusive flux later at the autumnal overturn period. Thermal structure might become even stronger in years of low precipitations such as in 2014, when concentrations of solutes (DOC, ions) increase through evaporation, intensifying density gradients thus GHG storage. Diffusive CH<sub>4</sub> fluxes were indeed statistically higher ( $p < 0.01$ ) in 2014 compared to 2013, although no such trend was observed for CO<sub>2</sub>.

The highest GHG saturation levels observed over the sampling period were measured in a trough pond the day following a major erosion event (peat block collapsing in pond BYL27; Fig. C1). This might result from the disturbance of the thermal structure and transfer of stored GHG to the surface, or from the causal effect of a new input of organic matter to microbial activity. Active shore erosion around tundra ponds, potentially increasing CH<sub>4</sub> production by 2 to 3 orders of magnitude, has been reported from similar systems in Siberia (Langer et al., 2015), suggesting a direct impact of permafrost slumping on GHG emissions. The effect of erosion events on GHG flux must be further evaluated as other factors, such as fluctuating wind and air temperature, can also influence mixing and surface GHG concentrations (Tedford et al., 2014).

Interestingly, we also observed substantial differences in GHG concentrations among trough ponds, some presenting much lower values. Trough ponds such as BYL24 (Fig. 2g) had relatively stable (non eroding) shores, and were colonized by abundant vegetation dominated by brown mosses. Methane oxidation by bacteria associated with submerged brown mosses has been reported in Siberian ponds, contributing to smaller CH<sub>4</sub> concentrations in these ecosystems (Liebner et al., 2011). Therefore, there might be cases where

the methanotrophic community is also efficient in limiting CH<sub>4</sub> emissions from trough ponds (Negandhi et al., 2014).

## 5.2 Production pathways of CO<sub>2</sub> and CH<sub>4</sub>

We obtained different radiocarbon ages for CO<sub>2</sub> and CH<sub>4</sub> within the same ebullition samples, as collected from funnels placed at the water surface (Table 2, Fig. 5), suggesting that GHG production was derived from different carbon sources. This divergence in carbon age was even more pronounced for the lakes, where it could reach almost 3000 years. The presence of unfrozen sediment layers (talik) underneath the lakes would explain the older bubbling CH<sub>4</sub> emitted from deeper and older sediments exposed to microbial degradation, as found in thermokarst lakes of Siberia and Alaska (Walter et al., 2007). Younger CO<sub>2</sub> could then be explained by a larger contribution of younger and shallower surface sediments to bacterial production and respiration. It could also result from lateral inputs of CO<sub>2</sub> produced within younger organic material or from exchanges with atmospheric CO<sub>2</sub>.

On the other hand, century-old CO<sub>2</sub> collected from ponds in parallel to modern CH<sub>4</sub> is more difficult to explain. As stated above, emission of young CH<sub>4</sub> suggests the preferential use of modern carbon by methanogens, and also a dominance of background ebullition mode (from surface sediments) in thaw ponds. Meanwhile, emission of older CO<sub>2</sub> could be related to anaerobic CO<sub>2</sub> production in water-saturated and reductive soils and its subsequent lateral transport, as observed in a flooded tundra site in Alaska (Zona et al., 2012). Characterizing organic matter properties and oxidation versus reduction (redox) potential of pond and lake sediments at our study sites are required to confirm if such a mechanism can contribute to modern CH<sub>4</sub> emissions from surface layers and, at the same time, older CO<sub>2</sub> emissions from deeper layers. Moreover, a quantification of lateral fluxes of carbon within the active layer (groundwater and streams), an important yet rarely mentioned process driven by the coupling between carbon and water cycles (Vonk and Gustafsson, 2013; Paytan et al., 2015), could help to better understand these results.

Notwithstanding the above-mentioned differences, the concentrations of CO<sub>2</sub> and CH<sub>4</sub> emitted through ebullition also need to be taken into account when evaluating the climate feedback potential of these emissions. Even though the age of CO<sub>2</sub> could reach several centuries (> 1000 yr BP for one sample; Fig. 5), it was 1 to 2 orders of magnitude less concentrated in the emitted bubbles than CH<sub>4</sub>. Hence, such emissions have a much lower potential to generate a positive feedback effect, at least during the ice-free season and under current climate conditions. Similar observations were reported from Siberian lakes, despite notably different geomorphological, geocryological and limnological conditions (Walter et al., 2007).

Methanogenesis in cold wetland systems typically proceeds via the anaerobic fermentation pathways of acetoclastic methanogenesis (AM) and/or hydrogenotrophic carbonate reduction methanogenesis (HM) (e.g., Kotsyurbenko et al., 2004; Alstad and Whiticar, 2011). AM utilizes the transfer of a CH<sub>3</sub><sup>-</sup> group from preformed organic substrates (i.e., acetate, methanol, methylated substrates, etc.), whereas HM utilizes H<sub>2</sub> and CO<sub>2</sub>. Numerous studies have demonstrated the ability of using methane C and H isotope signatures to discriminate AM from HM pathways, and to characterize secondarily altered methane (oxidation, mixing, etc.). Polygonal ponds and lakes had combined methane C and H stable isotope signatures that were typical for methanogenesis dominated by AM, as clearly illustrated in the plot of δ<sup>13</sup>CH<sub>4</sub> versus δDCH<sub>4</sub> (Fig. 7). Trough ponds shared similar δ<sup>13</sup>CH<sub>4</sub> values with the other water bodies, but had substantially more <sup>2</sup>H-depleted values (δDCH<sub>4</sub> from -398 to -448 ‰; Table 2, Fig. 7). These values are among the most <sup>2</sup>H-depleted values known for naturally occurring methane (e.g., Whiticar, 1999). Although there was some variation between sites, the isotope signatures designate that all CH<sub>4</sub> emitted by ebullition in July is produced by AM, consistent with an earlier study at the same site (Negandhi et al., 2013). There is no indication of HM, which has a very different isotope signature, although the signature of samples collected from the center of lakes tend to lie towards the HM region, suggesting that a small proportion of the CH<sub>4</sub> produced could be through this pathway. This finding of AM dominance is consistent with ombrotrophic bogs with higher pH (ranging from ~ 6.7 to 10.0 in 2014) compared with more acidic minerotrophic wetlands, which can be HM dominated (e.g., Bowes and Hornibrook, 2006; Prater et al., 2007). The dominance of AM is likely related to the carbon precursors; our sites may have more labile organic material present (e.g., organic acids) supporting acetoclastic methanogenesis and recently made available to methanogens. As this labile carbon pool is exhausted, the methanogenic pathway shifts from acetoclastic to more recalcitrant compounds and hence hydrogenotrophic methanogenesis (e.g., Alstad and Whiticar, 2011). It is therefore possible that other periods of the year would show a stronger HM signature, which would also be consistent with the presence of a large fraction of microbes able to perform HM in thaw ponds from this site (Negandhi et al., 2013).

Previous work in this valley indicated a significant relationship between water oxygen concentration and dissolved CH<sub>4</sub> oxidation level (Negandhi et al., 2013). This work also showed evidence that diffusive CH<sub>4</sub> was more susceptible to oxidation in polygonal ponds where a methanotrophic community was favored (Negandhi et al., 2014). This conclusion was supported by the strong shift in δ<sup>13</sup>CH<sub>4</sub> and δDCH<sub>4</sub> to the heavier isotopes, as expected (Whiticar et al., 1986). In the present study, there was no evidence of methane oxidation in any of the collected ebullition samples (Fig. 8), indicating that the conditions did not favor oxidation at the

**Table 4.** Greenhouse gas fluxes of CO<sub>2</sub> and CH<sub>4</sub> from high-latitude sites across the circum-Arctic. D = diffusion; E = ebullition.

Reference	Region	Type	Mode	CO <sub>2</sub>		CH <sub>4</sub>		Notes
				Min	Max	Min	Max	
Bouchard et al. (this study)	NE Canada	Polygon ponds	D + E	-141.4	741.1	0.5	6432.0	July measurements
		Troughs	D + E	-65.3	848.1	2.6	465.1	
		Lakes	D + E	-84.6	61.6	0.7	74.5	
Laurion et al. (2010)	NE Canada	Subarctic ponds	D	27.6	746.4	0.4	5.4	July measurements
		Arctic ponds	D	-246.0	1372.8	0.4	67.4	
		Arctic lakes	D	-63.6	70.8	0.1	0.4	
Buell (2015)	NW Canada	Ponds	D + E	-3.5	120.0			Headspace, chamber and flux tower methods
Kling et al. (1992)	Alaska	Lakes and rivers	D	-66.0	717.6	1.0	12.2	25 lakes + 4 rivers
Walter Anthony and Anthony 2013	Alaska	Thermokarst lakes	E			0.6	155.7	Strongest emissions = submerged polygons (lake shore)
Sepulveda-Jauregui et al. (2015)	Alaska	Lakes	D + E	51.9	2276.9	3.0	455.4	From annual fluxes, considering the ice-free period = 180 days
Walter-Anthony et al. (2010)	Alaska, Siberia	Thermokarst lakes	E			0.0	18 716.8	Background + seep ebullition
Abnizova et al. (2012)	Siberia	Whole landscape	D + E	200.0	1100.0			September measurements, flux tower
Blodau et al. (2008)	Siberia	Ponds	D	Average = 20.5		82.3	127.2	
Kankaala et al. (2013)	Finland	Lakes	D	140.0	1586.7	0.2	26.7	From annual fluxes, considering the ice-free period = 180 days
Huttunen et al. (2003)	Finland	Lakes and reservoirs	D + E	-21.6	876.0	0.8	99.6	
Bastviken et al. (2004)	Sweden	Lakes	D			0.6	11.0	From annual fluxes, considering the ice-free period = 180 days

production site (likely in anoxic sediment but also potentially in the water column; Grossart et al., 2011), and that the exchange with a pool of oxidized methane during the transport of bubbles to surface waters was undetectable, possibly linked to the short residence time. This was expected for shallow waters where bubbles can rapidly escape, but it was also the case in larger and deeper stratified lakes such as BYL36.

### 5.3 Bylot ponds and lakes within the circumpolar North

The general topography and geology of the southwest plain of Bylot, together with the distinct local conditions of the Qarlikturvik valley (e.g., glacier and outwash plain activity, valley orientation in relation to dominant winds, snow cover depth and density), have contributed to the development over thousands of years of what is arguably one of the richest ecosystems in the region. However, taken separately, most of the landscape features in the valley (e.g., tundra polygons, ice-wedges, thermokarst ponds and lakes) are widespread across the Arctic (e.g., Walter-Anthony et al., 2010; Abnizova et al., 2012; Langer et al., 2015). When compared with flux values reported in the literature, our results, representing a snapshot of mid-summer conditions, generally appear in the range of what has been observed in other ponds and lakes from northern regions (Ta-

ble 4). For example, we measured total CO<sub>2</sub> fluxes (diffusion + ebullition) of up to  $\sim 0.8 \text{ g C m}^{-2} \text{ d}^{-1}$ , which is in the range of those reported from Alaska (0.7–2.3  $\text{g C m}^{-2} \text{ d}^{-1}$ ; Kling et al., 1992; Sepulveda-Jauregui et al., 2015), Siberia (0.02–1.1  $\text{g C m}^{-2} \text{ d}^{-1}$ ; Abnizova et al. 2012; Blodau et al., 2008), and Scandinavia (0.9–1.6  $\text{g C m}^{-2} \text{ d}^{-1}$ ; Huttunen et al., 2003; Kankaala et al., 2013). Methane fluxes (diffusion + ebullition) at our study site varied substantially (0.0005–6.4  $\text{g C m}^{-2} \text{ d}^{-1}$ ), but could reach values 1 order of magnitude higher than those from lakes in Alaska (0.01–0.5  $\text{g C m}^{-2} \text{ d}^{-1}$ ; Kling et al., 1992; Sepulveda-Jauregui et al., 2015; Walter-Anthony and Anthony, 2013) and Scandinavia (0.01–0.1  $\text{g C m}^{-2} \text{ d}^{-1}$ ; Bastviken et al., 2004; Huttunen et al., 2003; Kankaala et al., 2013). However, median values for polygonal and trough ponds ( $\sim 0.02$  and  $0.01 \text{ g C m}^{-2} \text{ d}^{-1}$ , respectively) were more similar to published ranges. Yet, these fluxes were lower than those reported from Siberian thermokarst lakes in *yedoma* deposits (nearly  $20 \text{ g C m}^{-2} \text{ d}^{-1}$ ; Walter-Anthony et al., 2010), which however include discrete ebullition seeps and hotspots that were not observed in our study, and most likely do not exist in the case of ponds.

## 6 Conclusions

Aquatic systems are widespread across permafrost landscapes and play a crucial role in large-scale biogeochemical cycles. Yet, there is still much uncertainty about whether or not the Arctic can globally be considered a carbon source or sink, and how this will change in the coming decades. One element of such uncertainty is the highly heterogeneous distribution of ponds and lakes at the local scale and their different geomorphological and limnological properties, which influence their biogeochemistry and result in highly variable fluxes, especially for trough ponds. Our study demonstrates that local geomorphology and shoreline erosion around permafrost ponds and lakes can have a strong impact on their GHG concentrations and fluxes. We also report substantially different GHG ages among ponds and lakes of contrasting sizes and depths, and unexpectedly the emission of mainly modern CH<sub>4</sub> from trough ponds despite their exposure to a stock of eroding old carbon. Such results underscore the importance of the combined effects of geomorphology (talik development level, chronostratigraphy), limnology (or-

ganic matter concentration, CH<sub>4</sub> production and storage in anoxic/hypoxic bottom waters) and hydrology (lateral runoff inputs of organic material or GHG) on GHG emissions by permafrost thaw ponds and lakes. Interestingly, the significant correlation between GHG flux and DOM once more suggests the key role of this limnological characteristic, and calls for a deeper investigation as it could be used as a proxy for upscaling and modeling. The dominance of acetoclastic methanogenesis indicates that the system is presently rich in labile precursor substrates (e.g., acetate, formate, methylated substrates). However, the oldest CH<sub>4</sub> ages (~ 3.5 kyr BP) obtained from a thermokarst lake corresponded to the maximal age of the frozen organic (peat) layers in the valley, suggesting that permafrost thaw might have (or will soon have) proceeded through the organic substrate at this site. The local differences in surface areas, emissions rates, carbon age and sources reported in this study need to be further characterized in other regions of the Arctic in order to properly upscale and model GHG emissions and carbon-climate feedbacks across permafrost lake-rich landscapes.

## Appendix A



**Figure A1.** Picture of the homemade funnels deployed in ponds and lakes (photo taken in July 2014 just after their removal).

## Appendix B

**Table B1.** Temperature and total precipitation data for the 6 months preceding the sampling period in July 2013 and 2014. The climate normal (1981–2010) is also indicated (Environment Canada, 2015).

Month	Temperature (°C)			Precipitation (mm)		
	2013	2014	Normal	2013	2014	Normal
Jan	−28.7	−30.8	−33.4	13.4	1.5	4.8
Feb	−30.5	−32.7	−33.7	0.0	0.4	3.8
Mar	−22.2	−29.8	−30.0	22.0	0.0	6.6
Apr	−19.5	−19.8	−21.8	14.2	1.6	10.5
May	−12.4	−7.2	−9.3	0.0	17.6	9.4
Jun	3.4	2.5	2.4	20.7	5.9	15.6
Total (Jan–Jun)	−18.3	−19.6	−21.0	70.3	27.0	50.7

## Appendix C



**Figure C1.** Picture of eroding shores (slumping peat) along trough pond BYL27 (photo taken in July 2014). The sampling funnel syringe can be seen just above the water surface.

## Appendix D

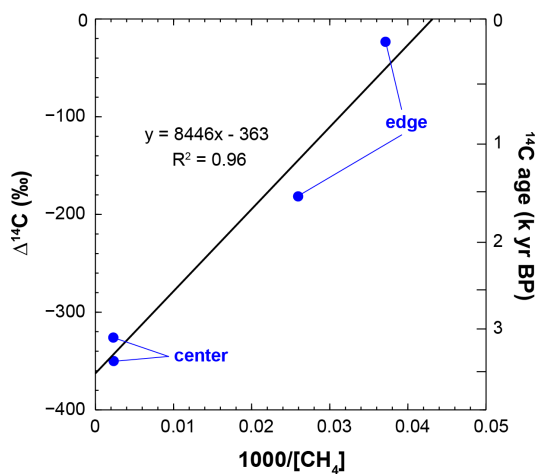


**Figure D1.** Keeling plot of lake ebullition  $\text{CH}_4$  sampled in 2014, showing a mixing of millennium-old and highly concentrated gas with near-modern and less concentrated gas. Concentration ( $x$  axis) is expressed as  $1000/\text{partial pressure}$  (in ppmv, parts per million volumetric), whereas radiocarbon age is expressed as the normalized radiocarbon activity ( $\Delta^{14}\text{C}$ , in ‰; left  $y$  axis) and in thousands of years before present (kyr BP; right  $y$  axis).

*Author contributions.* F. Bouchard, I. Laurion and V. Prèskienis designed the experiments, and F. Bouchard and V. Prèskienis performed them. I. Laurion, D. Fortier, X. Xu and M. J. Whiticar contributed materials, instruments and analyses. F. Bouchard, I. Laurion, V. Prèskienis and D. Fortier analyzed the data. F. Bouchard prepared the manuscript with contributions from all co-authors.

*Acknowledgements.* We are grateful to H. White, G. Lupiens, D. Sarrazin and the team of G. Gauthier (U. Laval) for their help in the field, and to J. Vonk, R. Tremblay, M. Langer and an anonymous referee for their helpful comments on an earlier version of the manuscript. We also thank the Pond Inlet (Mittimatalik) community, the Center for Northern Studies (CEN) and Parks Canada (Sirmilik National Park) for logistical support and access to the study site. This project was funded by ArcticNet, the Natural Sciences and Engineering Research Council of Canada (NSERC), the Polar Continental Shelf Program (PCSP) of Natural Resources Canada, the NSERC Discovery Frontiers grant “Arctic Development and Adaptation to Permafrost in Transition” (ADAPT), the EnviroNorth Training Program, and the W. Garfield Weston Foundation.

Edited by: J. Vonk

## References

- Abnizova, A., Siemens, J., Langer, M., and Boike, J.: Small ponds with major impact: The relevance of ponds and lakes in permafrost landscapes to carbon dioxide emissions, *Global Biogeochem. Cycles*, 26, doi:10.1029/2011gb004237, 2012.
- Allard, M.: Geomorphological changes and permafrost dynamics: Key factors in changing arctic ecosystems. An example from Bylot Island, Nunavut, Canada, *Geoscience Canada*, 23, 205–212, 1996.
- Alstad, K. P. and Whiticar, M. J.: Carbon and hydrogen isotope ratio characterization of methane dynamics for Fluxnet Peatland Ecosystems, *Org. Geochem.*, 42, 548–558, doi:10.1016/j.orggeochem.2011.03.004, 2011.
- Bastviken, D., Cole, J., Pace, M., and Tranvik, L.: Methane emissions from lakes: Dependence of lake characteristics, two regional assessments, and a global estimate, *Global Biogeochem. Cycles*, 18, GB4009, doi:10.1029/2004GB002238, 2004.
- Bastviken, D., Cole, J. J., Pace, M. L., and Van de Bogert, M. C.: Fates of methane from different lake habitats: Connecting whole-lake budgets and CH<sub>4</sub> emissions, *J. Geophys. Res.-Biogeosciences*, 113, 13, doi:10.1029/2007jg000608, 2008.
- Blodau, C., Rees, R., Flessa, H., Rodionov, A., Guggenberger, G., Knorr, K. H., Shibistova, O., Zrazhevskaya, G., Mikheeva, N., and Kasansky, O. A.: A snapshot of CO<sub>2</sub> and CH<sub>4</sub> evolution in a thermokarst pond near Igarka, northern Siberia, *J. Geophys. Res.-Biogeosciences*, 113, G03023, doi:10.1029/2007jg000652, 2008.
- Boereboom, T., Depoorter, M., Coppens, S., and Tison, J.-L.: Gas properties of winter lake ice in Northern Sweden: implication for carbon gas release, *Biogeosciences*, 9, 827–838, doi:10.5194/bg-9-827-2012, 2012.
- Bostock, H. S.: Physiographic subdivisions of Canada, in: *Geology and economic minerals of Canada. Economic Geology Report No. 1.*, edited by: Douglas, R. J. W., Geological Survey of Canada, Ottawa, 9–30, 1970.
- Bouchard, F., Fortier, D., Paquette, M., Bégin, P. N., Vincent, W. F., and Laurion, I.: Lake bottom imagery: a simple, fast and inexpensive method for surveying shallow freshwater ecosystems of permafrost regions, *Proceedings of the 7th Canadian Permafrost Conference and the 68th Canadian Geotechnical Conference*, Quebec City, 20–23 September 2015.
- Bowes, H. L. and Hornibrook, E. R. C.: Emission of highly <sup>13</sup>C-depleted methane from an upland blanket mire, *Geophys. Res. Lett.*, 33, L04401, doi:10.1029/2005GL025209, 2006.
- Brosius, L. S., Walter Anthony, K. M., Grosse, G., Chanton, J. P., Farquharson, L. M., Overduin, P. P., and Meyer, H.: Using the deuterium isotope composition of permafrost meltwater to constrain thermokarst lake contributions to atmospheric CH<sub>4</sub> during the last deglaciation, *J. Geophys. Res.-Biogeosciences*, 117, G01022, doi:10.1029/2011jg001810, 2012.
- Brown, J., Ferrians, O. J., Heginbottom, J. A., and Melnikov, E. S.: *Circum-Arctic map of permafrost and ground-ice conditions*, National Snow and Ice Data Center/World Data Center for Glaciology, Boulder, Colorado, 1998.
- Buell, M.-C.: CO<sub>2</sub> dynamics of tundra ponds in the low-Arctic, Northwest Territories, Canada, MS Thesis, *Environmental Resource Sciences*, Trent University, 104 p., 2015.
- Burn, C. R. and Kokelj, S. V.: The environment and permafrost of the Mackenzie Delta area, *Permafrost Periglac.*, 20, 83–105, doi:10.1002/ppp.655, 2009.
- CEN: Environmental data from Bylot Island in Nunavut, Canada, v. 1.4 (1992–2014), *Nordicana D2*, last access: 20 March 2015, doi:10.5885/45039SL-EE76C1BDAADC4890, 2014.
- Cole, J. J. and Caraco, N. F.: Atmospheric exchange of carbon dioxide in a low-wind oligotrophic lake measured by the addition of SF<sub>6</sub>, *Limnol. Oceanogr.*, 43, 647–656, 1998.
- Duclos, I.: Milieux mésiques et secs de l’île Bylot, Nunavut (Canada): caractérisation et utilisation par la grande oie des neiges, MSc thesis, Université du Québec à Trois-Rivières (UQTR), 115 p., 2002.
- Dyke, A. S. and Prest, V. K.: Late Wisconsinan and Holocene History of the Laurentide Ice Sheet, *Géographie physique et Quaternaire*, 41, 237–263, 1987.
- Ellis, C. J., Rochefort, L., Gauthier, G., and Pienitz, R.: Paleogeological Evidence for Transitions between Contrasting Landforms in a Polygon-Patterned High Arctic Wetland, *Arctic, Antarctic, Alpine Res.*, 40, 624–637, doi:10.1657/1523-0430(07-059)[ellis]2.0.co;2, 2008.
- Environment Canada: 1981–2010 Climate Normals & Averages, [http://climate.weather.gc.ca/climate\\_normals/index\\_e.html](http://climate.weather.gc.ca/climate_normals/index_e.html), last access: 10 February 2015.
- Fortier, D. and Allard, M.: Late Holocene syngenetic ice-wedge polygons development, Bylot Island, Canadian Arctic Archipelago, *Can. J. Earth Sci.*, 41, 997–1012, doi:10.1139/e04-031, 2004.
- Fortier, D., Allard, M., and Pivot, F.: A late-Holocene record of loess deposition in ice-wedge polygons reflecting wind activity and ground moisture conditions, *Bylot Island, eastern Canadian Arctic, Holocene*, 16, 635–646, doi:10.1191/0959683606hl960rp, 2006.

- Gao, X., Schlosser, C. A., Sokolov, A., Walter Anthony, K. W., Zhuang, Q. L., and Kicklighter, D.: Permafrost degradation and methane: low risk of biogeochemical climate-warming feedback, *Environ. Res. Lett.*, 8, 035014, doi:10.1088/1748-9326/8/3/035014, 2013.
- Godin, E., Fortier, D., and Coulombe, S.: Effects of thermo-erosion gullyng on hydrologic flow networks, discharge and soil loss, *Environ. Res. Lett.*, 9, 105010, doi:10.1088/1748-9326/9/10/105010, 2014.
- Grossart, H.-P., Frindte, K., Dziallas, C., Eckert, W., and Tang, K. W.: Microbial methane production in oxygenated water column of an oligotrophic lake, *P. Natl. Acad. Sci. USA*, 108, 19657–19661, doi:10.1073/pnas.1110716108, 2011.
- Grosse, G., Jones, B., and Arp, C.: Thermokarst Lakes, Drainage, and Drained Basins, in: *Treatise on Geomorphology*, edited by: Shroder, J. F., *Glacial and Periglacial Geomorphology*, 8, Academic Press, San Diego, CA, 325–353, 2013.
- Guo, L., Ping, C.-L., and Macdonald, R. W.: Mobilization pathways of organic carbon from permafrost to arctic rivers in a changing climate, *Geophys. Res. Lett.*, 34, L13603, doi:10.1029/2007GL030689, 2007.
- Hesslein, R. H., Rudd, J. W. M., Kelly, C. A., Ramlal, P., and Hallard, K. A.: Carbon dioxide pressure in surface waters of Canadian lakes, in: *Air-water mass transfer*, edited by: Wilhelms, S. C. and Gulliver, J. S., American Society of Civil Engineers, New York, 413–431, 1991.
- Hugelius, G., Strauss, J., Zubrzycki, S., Harden, J. W., Schuur, E. A. G., Ping, C.-L., Schirmermeister, L., Grosse, G., Michaelson, G. J., Koven, C. D., O'Donnell, J. A., Elberling, B., Mishra, U., Camill, P., Yu, Z., Palmtag, J., and Kuhry, P.: Estimated stocks of circumpolar permafrost carbon with quantified uncertainty ranges and identified data gaps, *Biogeosciences*, 11, 6573–6593, doi:10.5194/bg-11-6573-2014, 2014.
- Huttunen, J. T., Alm, J., Liikanen, A., Juutinen, S., Larmola, T., Hammar, T., Silvola, J., and Martikainen, P. J.: Fluxes of methane, carbon dioxide and nitrous oxide in boreal lakes and potential anthropogenic effects on the aquatic greenhouse gas emissions, *Chemosphere*, 52, 609–621, doi:10.1016/S0045-6535(03)00243-1, 2003.
- IPCC: Changes in Atmospheric Constituents and in Radiative Forcing, in: *Climate Change 2007: The Physical Science Basis. Contribution of Working Group I to the Fourth Assessment Report of the Intergovernmental Panel on Climate Change*, edited by: Solomon, S., Qin, D., Manning, M., Chen, Z., Marquis, M., Averyt, K. B., Tignor, M., and Miller, H. L., Cambridge University Press, Cambridge, UK, 2007.
- Kankaala, P., Huotari, J., Tulonen, T., and Ojala, A.: Lake-size dependent physical forcing drives carbon dioxide and methane effluxes from lakes in a boreal landscape, *Limnol. Oceanogr.*, 58, 1915–1930, doi:10.4319/lo.2013.58.6.1915, 2013.
- Klassen, R. A.: Quaternary Geology and Glacial History of Bylot Island, Northwest Territories, Geological Survey of Canada, Ottawa, 1993.
- Kling, G. W., Kipphut, G. W., and Miller, M. C.: The flux of CO<sub>2</sub> and CH<sub>4</sub> from lakes and rivers in arctic Alaska, *Hydrobiologia*, 240, 23–36, doi:10.1007/bf00013449, 1992.
- Kotsyurbenko, O. R., Chin, K.-J., Glagolev, M. V., Stubner, S., Simankova, M. V., Nozhevnikova, A. N., and Conrad, R.: Acetoclastic and hydrogenotrophic methane production and methanogenic populations in an acidic West-Siberian peat bog, *Environ. Microbiol.*, 6, 1159–1173, doi:10.1111/j.1462-2920.2004.00634.x, 2004.
- Kutzbach, L., Wille, C., and Pfeiffer, E.-M.: The exchange of carbon dioxide between wet arctic tundra and the atmosphere at the Lena River Delta, Northern Siberia, *Biogeosciences*, 4, 869–890, doi:10.5194/bg-4-869-2007, 2007.
- Lamoureux, S. F. and Lafrenière, M. J.: Seasonal fluxes and age of particulate organic carbon exported from Arctic catchments impacted by localized permafrost slope disturbances, *Environ. Res. Lett.*, 9, 045002, doi:10.1088/1748-9326/9/4/045002, 2014.
- Langer, M., Westermann, S., Walter Anthony, K., Wischniewski, K., and Boike, J.: Frozen ponds: production and storage of methane during the Arctic winter in a lowland tundra landscape in northern Siberia, Lena River delta, *Biogeosciences*, 12, 977–990, doi:10.5194/bg-12-977-2015, 2015.
- Lauriol, B., Lacelle, D., St-Jean, M., Clark, I. D., and Zazula, G. D.: Late Quaternary paleoenvironments and growth of intrusive ice in eastern Beringia (Eagle River valley, northern Yukon, Canada), *Can. J. Earth Sci.*, 47, 941–955, doi:10.1139/e10-012, 2010.
- Laurion, I. and Mladenov, N.: Dissolved organic matter photolysis in Canadian arctic thaw ponds, *Environ. Res. Lett.*, 8, 035026, doi:10.1088/1748-9326/8/3/035026, 2013.
- Laurion, I., Vincent, W. F., MacIntyre, S., Retamal, L., Dupont, C., Francus, P., and Pienitz, R.: Variability in greenhouse gas emissions from permafrost thaw ponds, *Limnol. Oceanogr.*, 55, 115–133, doi:10.4319/lo.2010.55.1.0115, 2010.
- Liebner, S., Zeyer, J., Wagner, D., Schubert, C., Pfeiffer, E. M., and Knoblauch, C.: Methane oxidation associated with submerged brown mosses reduces methane emissions from Siberian polygonal tundra, *J. Ecology*, 99, 914–922, doi:10.1111/j.1365-2745.2011.01823.x, 2011.
- Mann, P. J., Eglinton, T. I., McIntyre, C. P., Zimov, N., Davydova, A., Vonk, J. E., Holmes, R. M., and Spencer, R. G. M.: Utilization of ancient permafrost carbon in headwaters of Arctic fluvial networks, *Nature Communications*, 6, 7856, doi:10.1038/ncomms8856, 2015.
- Myhre, G., Shindell, D., Bréon, F.-M., Collins, W., Fuglestedt, J., Huang, J., Koch, D., Lamarque, J.-F., Lee, D., Mendoza, B., Nakajima, T., Robock, A., Stephens, G., Takemura, T., and Zhang, H.: Anthropogenic and Natural Radiative Forcing, in: *Climate Change 2013: The Physical Science Basis. Contribution of Working Group I to the Fifth Assessment Report of the Intergovernmental Panel on Climate Change*, edited by: Stocker, T. F., Qin, D., Plattner, G.-K., Tignor, M., Allen, S. K., Boschung, J., Nauels, A., Xia, Y., Bex, V., and Midgley, P. M., Cambridge University Press, Cambridge (UK) and New York (USA), 659–740, doi:10.1017/CBO9781107415324.018, 2013.
- Negandhi, K.: Defining water sources and extent of evaporation of arctic thermokarst (thaw) ponds using water isotope tracers, Institut national de la recherche scientifique (INRS), Centre Eau Terre Environnement (ETE), Scientific and Technical Document No. I357, Québec City, 2013.
- Negandhi, K., Laurion, I., Whiticar, M. J., Galand, P. E., Xu, X., and Lovejoy, C.: Small Thaw Ponds: An Unaccounted Source of Methane in the Canadian High Arctic, *Plos One*, 8, e78204, doi:10.1371/journal.pone.0078204, 2013.

- Negandhi, K., Laurion, I., and Lovejoy, C.: Bacterial communities and greenhouse gas emissions of shallow ponds in the High Arctic, *Polar Biology*, 37, 1669–1683, doi:10.1007/s00300-014-1555-1, 2014.
- Pack, M. A., Xu, X., Lupascu, M., Kessler, J. D., and Czimczik, C. I.: A rapid method for preparing low volume CH<sub>4</sub> and CO<sub>2</sub> gas samples for 14C AMS analysis, *Org. Geochem.*, 78, 89–98, doi:10.1016/j.orggeochem.2014.10.010, 2015.
- Parks Canada: Sirmilik National Park of Canada, <http://www.pc.gc.ca/eng/pn-np/nu/sirmilik/index.aspx>, last access: 10 February 2014.
- Paytan, A., Lecher, A. L., Dimova, N., Sparrow, K. J., Kodovska, F. G.-T., Murray, J., Tulaczyk, S., and Kessler, J. D.: Methane transport from the active layer to lakes in the Arctic using Toolik Lake, Alaska, as a case study, *P. Natl. Acad. Sci. USA*, 112, 3636–3640, doi:10.1073/pnas.1417392112, 2015.
- Prater, J. L., Chanton, J. P., and Whiting, G. J.: Variation in methane production pathways associated with permafrost decomposition in collapse scar bogs of Alberta, Canada, *Global Biogeochem. Cycles*, 21, GB4004, doi:10.1029/2006GB002866, 2007.
- Reimer, P. J., Brown, T. A., and Reimer, R. W.: Discussion: Reporting and Calibration of Post-Bomb 14C Data, *Radiocarbon*, 46, 1299–1304, 2004.
- Roiha, T., Laurion, I., and Rautio, M.: Carbon dynamics in highly heterotrophic subarctic thaw ponds, *Biogeosciences Discuss.*, 12, 11707–11749, doi:10.5194/bgd-12-11707-2015, 2015.
- Romanovsky, V. E., Smith, S. L., and Christiansen, H. H.: Permafrost thermal state in the polar Northern Hemisphere during the international polar year 2007–2009: a synthesis, *Permafrost Periglac.*, 21, 106–116, doi:10.1002/ppp.689, 2010.
- Schuur, E. A. G., McGuire, A. D., Schadel, C., Grosse, G., Harden, J. W., Hayes, D. J., Hugelius, G., Koven, C. D., Kuhry, P., Lawrence, D. M., Natali, S. M., Olefeldt, D., Romanovsky, V. E., Schaefer, K., Turetsky, M. R., Treat, C. C., and Vonk, J. E.: Climate change and the permafrost carbon feedback, *Nature*, 520, 171–179, doi:10.1038/nature14338, 2015.
- Sepulveda-Jauregui, A., Walter Anthony, K. M., Martinez-Cruz, K., Greene, S., and Thalasso, F.: Methane and carbon dioxide emissions from 40 lakes along a north–south latitudinal transect in Alaska, *Biogeosciences*, 12, 3197–3223, doi:10.5194/bg-12-3197-2015, 2015.
- Smith, S. and Burgess, M. M.: Ground Temperature Database for Northern Canada, Geological Survey of Canada, Ottawa, Open File Report 3954, 28 p., 2000.
- Southon, J. and Santos, G. M.: Life with MC-SNICS. Part II: Further ion source development at the Keck carbon cycle AMS facility, *Nuclear Instruments and Methods in Physics Research Section B: Beam Interactions with Materials and Atoms*, 259, 88–93, doi:10.1016/j.nimb.2007.01.147, 2007.
- Stainton, M. P., Capel, M. J., and Armstrong, F. A. J.: The chemical analysis of fresh water, 2nd Ed., Serv., C. F. M., Misc. Spec. Publ., 25, 1977.
- Stepanenko, V. M., Machul'skaya, E. E., Glagolev, M. V., and Lykossov, V. N.: Numerical Modeling of Methane Emissions from Lakes in the Permafrost Zone, *Izv. Atmos. Ocean. Phys.*, 47, 252–264, doi:10.1134/s0001433811020113, 2011.
- Stuiver, M., and Polach, H. A.: Discussion: reporting 14C data, *Radiocarbon*, 19, 355–363, 1977.
- Tarnocai, C., Canadell, J. G., Schuur, E. A. G., Kuhry, P., Mazhitova, G., and Zimov, S.: Soil organic carbon pools in the northern circumpolar permafrost region, *Global Biogeochem. Cycles*, 23, GB2023, doi:10.1029/2008GB003327, 2009.
- Tedford, E. W., MacIntyre, S., Miller, S. D., and Czikowsky, M. J.: Similarity scaling of turbulence in a temperate lake during fall cooling, *J. Geophys. Res.-Oceans*, 119, 4689–4713, doi:10.1002/2014JC010135, 2014.
- Tremblay, S., Bhiry, N., and Lavoie, M.: Long-term dynamics of a palsa in the sporadic permafrost zone of northwestern Quebec (Canada), *Can. J. Earth Sci.*, 51, 500–509, doi:10.1139/cjes-2013-0123, 2014.
- van Huissteden, J., Berrittella, C., Parmentier, F. J. W., Mi, Y., Maximov, T. C., and Dolman, A. J.: Methane emissions from permafrost thaw lakes limited by lake drainage, *Nat. Clim. Chang.*, 1, 119–123, doi:10.1038/nclimate1101, 2011.
- Vonk, J. E. and Gustafsson, O.: Permafrost-carbon complexities, *Nature Geoscience*, 6, 675–676, doi:10.1038/ngeo1937, 2013.
- Vonk, J. E., Mann, P. J., Davydov, S., Davydova, A., Spencer, R. G. M., Schade, J., Sobczak, W. V., Zimov, N., Zimov, S., Bulygina, E., Eglinton, T. I., and Holmes, R. M.: High biolability of ancient permafrost carbon upon thaw, *Geophys. Res. Lett.*, 40, 2689–2693, doi:10.1002/grl.50348, 2013.
- Vonk, J. E., Tank, S. E., Bowden, W. B., Laurion, I., Vincent, W. F., Alekseychik, P., Amyot, M., Billet, M. F., Canário, J., Cory, R. M., D eshpande, B. N., Helbig, M., Jammet, M., Karlsson, J., Larouche, J., MacMillan, G., Rautio, M., Walter Anthony, K. M., and Wickland, K. P.: Reviews and Syntheses: Effects of permafrost thaw on arctic aquatic ecosystems, *Biogeosciences Discuss.*, 12, 10719–10815, doi:10.5194/bgd-12-10719-2015, 2015.
- Walter, K. M., Zimov, S. A., Chanton, J. P., Verbyla, D., and Chapin, F. S.: Methane bubbling from Siberian thaw lakes as a positive feedback to climate warming, *Nature*, 443, 71–75, doi:10.1038/nature05040, 2006.
- Walter, K. M., Smith, L. C., and Chapin, F. S.: Methane bubbling from northern lakes: present and future contributions to the global methane budget, *Philos. T. R. Soc. A-Mathematical Physical and Engineering Sciences*, 365, 1657–1676, doi:10.1098/rsta.2007.2036, 2007.
- Walter, K. M., Chanton, J. P., Chapin, F. S., Schuur, E. A. G., and Zimov, S. A.: Methane production and bubble emissions from arctic lakes: Isotopic implications for source pathways and ages, *J. Geophys. Res.-Biogeosciences*, 113, G00A08, doi:10.1029/2007jg000569, 2008.
- Walter-Anthony, K. M. and Anthony, P.: Constraining spatial variability of methane ebullition seeps in thermokarst lakes using point process models, *J. Geophys. Res.-Biogeosciences*, 118, 1015–1034, doi:10.1002/jgrg.20087, 2013.
- Walter-Anthony, K. M., Vas, D. A., Brosius, L., Chapin, F. S., Zimov, S. A., and Zhuang, Q. L.: Estimating methane emissions from northern lakes using ice-bubble surveys, *Limnol. Oceanogr-Methods*, 8, 592–609, doi:10.4319/lom.2010.8.0592, 2010.
- Wanninkhof, R.: Relationship between wind-speed and gas-exchange over the ocean, *J. Geophys. Res.-Oceans*, 97, 7373–7382, doi:10.1029/92jc00188, 1992.
- Whiticar, M. J.: Carbon and hydrogen isotope systematics of bacterial formation and oxidation of methane, *Chemical Geology*, 161, 291–314, doi:10.1016/S0009-2541(99)00092-3, 1999.

- Whiticar, M. J., Faber, E., and Schoell, M.: Biogenic methane formation in marine and freshwater environments: CO<sub>2</sub> reduction vs. acetate fermentation—*isotope evidence*, *Geochim. Cosmochim. Ac.*, 50, 693–709, doi:10.1016/0016-7037(86)90346-7, 1986.
- Wik, M., Crill, P. M., Bastviken, D., Danielsson, A., and Norback, E.: Bubbles trapped in arctic lake ice: Potential implications for methane emissions, *J. Geophys. Res.-Biogeosciences*, 116, 10, doi:10.1029/2011jg001761, 2011.
- Wik, M., Crill, P. M., Varner, R. K., and Bastviken, D.: Multi-year measurements of ebullitive methane flux from three sub-arctic lakes, *J. Geophys. Res.-Biogeosciences*, 118, 1307–1321, doi:10.1002/jgrg.20103, 2013.
- Xu, X., Trumbore, S. E., Zheng, S., Southon, J. R., McDuffee, K. E., Luttgen, M., and Liu, J. C.: Modifying a sealed tube zinc reduction method for preparation of AMS graphite targets: Reducing background and attaining high precision, *Nuclear Instruments and Methods in Physics Research Section B: Beam Interactions with Materials and Atoms*, 259, 320–329, doi:10.1016/j.nimb.2007.01.175, 2007.
- Zimov, S. A., Voropaev, Y. V., Semiletov, I. P., Davidov, S. P., Prosiannikov, S. F., Chapin, F. S., Chapin, M. C., Trumbore, S., and Tyler, S.: North Siberian Lakes: A Methane Source Fueled by Pleistocene Carbon, *Science*, 277, 800–802, doi:10.1126/science.277.5327.800, 1997.
- Zimov, S. A., Schuur, E. A. G., and Chapin, F. S.: Permafrost and the Global Carbon Budget, *Science*, 312, 1612–1613, doi:10.1126/science.1128908, 2006.
- Zona, D., Lipson, D. A., Paw, K. T., Oberbauer, S. F., Olivas, P., Gioli, B., and Oechel, W. C.: Increased CO<sub>2</sub> loss from vegetated drained lake tundra ecosystems due to flooding, *Global Biogeochem. Cycles*, 26, GB2004, doi:10.1029/2011gb004037, 2012.